Journal Name

ARTICLE

Recent progress in covalent organic framework thin films: fabrications, applications and perspectives

Received 00th January 20xx,
Accepted 00th January 20xx

DOI: 10.1039/x0xx00000x

www.rsc.org/

Han Wang, †[a] Zhuotong Zeng, †[b] Piao Xu, †[a] Lianshan Li, †[c] Guangming Zeng,*[a] Rong Xiao,*[b] Zhiyong Tang,*[c] Danlian Huang,[a] Lin Tang,[a] Cui Lai,[a] Danni Jiang,[a] Yang Liu,[a] Huan Yi,[a] Lei Qin,[a] Shujing Ye,[a] Xiaoya Ren [a] and Wangwang Tang [a]

As a newly emerging class of porous material, covalent organic frameworks (COFs) have attracted much attention due to their intriguing structural merits (e.g., total organic backbone, tunable porosity and predictable structure). However, the insoluble and unprocessable features of the bulk COF powders limit their applications. To overcome these limitations, considerable efforts have been devoted to exploring the fabrication of COF thin films with controllable architectures and opening the door for their novel applications. In this critical review, we aim to provide recent advances in the fabrications of COF thin films not only supported on substrates but also acted as free-standing nanosheets by both bottom-up and top-down strategies. The bottom-up strategy contains solvothermal synthesis, interfacial polymerization, room temperature vapor-assisted conversion, and synthesis under continuous flow conditions, while the top-down strategy contains solvent-assisted exfoliation, self-exfoliation, mechanical delamination, and chemical exfoliation. In addition, the applications of COF thin films including energy storage,semiconductor devices, membrane-separation, sensors, and drug delivery are summarized. Finally, to speed up further research, a personal perspective covering synthetic strategies, mechanisms and applications is presented.

1. Introduction

For decades, porous materials have attracted sustained attention due to their abundant voids containing structure which enables them to host other functional molecules.[1-5] Owing to their unique features, porous organic materials, such as hypercrosslinked polymers (HCPs),[6, 7] conjugated microporous polymers (CMPs),[8-10] and porous aromatic frameworks (PAF),[11-13] have been widely studied. However, constructing persistent porous structure linked by covalent bonds is still a complicated problem in spite of that some remarkable progress have been made these years.[14-16] Crystalline networks with ordered pores are urgently in need. Covalent organic frameworks (COFs), as a class of newly emerging porous material, have attracted particular interests. Quite different from classical short-range covalent polymers connected via irreversible condensation,[17] COFs show highly ordered crystalline structures through reversible reactions.[18] Compared to the traditional crystalline porous solids such as zeolites[19, 20] and metal-organic frameworks (MOFs)[21-23], COFs with precisely pre-designable structures and tailored functionalities are able to achieve structural and chemical control that are specific to functions.[24] Moreover, they possess the advantages of structural diversity,[25] low density,[26] high thermal stability,[27, 28] and permanent porosity.[29]

In 2005, Yaghi and co-workers, for the first time, synthesized a type of pure two-dimensional (2D) organic frameworks, namely COF-1 and COF-5, which are composed of organic building subunits connected through strong covalent bonds by reticular chemistry.[30] Afterward, a great variety of COFs have sprung up including imine-linked COFs,[31-34] hydrazone-linked COFs,[35, 36] and keto-enol-linked COFs (Fig. 1).[37-39] Their abovementioned unique characters as well as common natures of organic polymers endow them great application potential in energy storage,[40-42] drug delivery,[43, 44] adsorption,[45, 46] separation,[47] catalysis,[48] optoelectronics,[49, 50] and sensing.[51] However, all of these applications are currently established on the basis of insoluble and unprocessable COF powders. Early in 2007, Kitagawa and Matsuda demonstrated that porous polymers are insoluble and difficult to be prepared into thin layers in spite of furnished nanosized channels or cavities.[52] The ultimate goal is to construct various nanodevices with controllable arrangements of porous modules' channels. Indeed, the difficulties in membrane formation greatly hinder the practical applications of COFs. For example, an anthraquinone based COF powder was incorporated into carbon black to act as an electrode material leading to a higher capacitance compared with that of electrode without COF

[a] College of Environmental Science and Engineering, Hunan University and Key Laboratory of Environmental Biology and Pollution Control (Hunan University), Ministry of Education, Changsha 410082, P. R. China. E-mail: zgming@hnu.edu.cn
[b] Department of Dermatology, Second Xiangya Hospital, Central South University, Changsha 410011, P. R. China. E-mail: xiaorong65@csu.edu.cn
[c] CAS Key Laboratory of Nanosystem and Hierachical Fabrication, CAS center for Excellent in Nanoscience, National Center for Nanoscience and Technology, Beijing 100190, P.R. China. E-mail: zytang@nanoctr.cn
† These authors contribute equally to this article.
Electronic Supplementary Information (ESI) available: [details of any supplementary information available should be included here]. See DOI: 10.1039/x0xx00000x

loading, whereas only 2.5 % of diaminoanthraquinone (DAAQ) moieties were available in the system because of the random oriented COF powders and non-optimal interface.[38] Thus, new strategies that can fabricate COFs into crystalline and ordered thin films are highly required for their further practical applications.

The bottom-up approach is the first important strategy that enables COFs to be deposited on specific substrates or polymerized at interface with controllable thickness and surface. Dichtel and co-workers pioneered the research on COF films growth on single-layer graphene (SLG) via a bottom-up method under solvothermal conditions.[53] The as-prepared COF films exhibited improved crystallinity over bulk COF powders, which are ideal for organic electronic devices. This intriguing research has opened the door for COF thin films fabrication. Since then, several innovative or modified methods for COF-film growth related to bottom-up strategy have been employed and oriented thin films supported by various substrates have been obtained. By now, four major methods have been used for the fabrication of COF thin films on different substrates or at interfaces: (1) solvothermal synthesis, (2) interfacial polymerization, (3) synthesis under continuous flow conditions, and (4) room temperature vapor-assisted conversion. All of these strategies will be discussed in detail in Section 2.

Another attractive method is top-down synthesis, which bulk COF powders are directly exfoliated into free-standing COF films, namely COF nanosheets (CONs). As we know, dimensionality is one of the most important parameters that affects the materials properties.[54, 55] Bulk lamellar COFs are stacked by atomic thick layers via weak van der Waals forces. Inspired by the excellent properties of graphene which is exfoliated from its parent graphite,[56-58] Félix Zamora group first exfoliated COF-8 into CONs with the thickness down to 1~8 nm.[59] The dimension related properties enable the thin layered COF-8 nanosheets to be incorporated into devices or act as nanosensors. After that, various functional CONs have been delaminated from their bulk counterparts by various methods such as solvent-assisted exfoliation, mechanical delamination, and self-exfoliation. All these different ways will be discussed comprehensively in the following.

Though there are many critical reviews focused on reticular chemistry of COF powders,[60-65] the review related to COF thin films is rare. In this review article, we focus on the recent developments on the fabrication of COF thin films supported not only on the substrate but also as free-standing forms. First, we summarized the synthesis strategies related to bottom-up and top-down method. Second, we discussed the existing applications of thin films in different fields such as energy storage, semiconductor devices, membrane-separation and sensors. Finally, we demonstrated a personal perspective regarding to the future development. It is worth mentioning that since the development of single-layered COF has been recently reviewed,[66] we focus on few layered COF thin films and exfoliated CONs in this article by collecting recent important developments in this exciting field and presenting critical issues, challenges, and perspectives.

The following Fig. 2 and 3 will be used to guide the readers to better understand the monomers and reversible reactions utilized for the construction of COF thin films.

2. Bottom-up strategy for the fabrication of COF thin films

As stated above, the excellent properties and imperious demands of COF thin films have triggered substantial research interests for their synthesis. Bottom-up strategy, which is usually related to the functional coatings on selected surface, has been widely used in COF thin film fabrications. The key of this strategy is to control the growth orientation of the film and avoid random extension. Up to now, a number of highly oriented COF thin films have been synthesized on various substrates or interfaces by bottom-up strategy. However, finding appropriate synthetic conditions for the COF thin films growth is not easy. Generally, solvothermal synthesis is the most frequently utilized method for flat COF thin films production. And other brilliant methods have also been employed containing interfacial synthesis, room temperature vapor-assisted conversion, and synthesis under continuous flow conditions. In this section, we will summarize these approaches based on existing studies.

2.1 Solvothermal synthesis

As a simplest method, solvothermal synthesis is to coat COF powders on arbitrary support by immersing proper substrates into a COF reaction mixture, followed by washing with related organic solvents and drying under a stream of N_2. The first successful production of continuous COF thin films was achieved on the basis of the traditional COF synthesis route by using solvothermal method, which put no specific requirements on the surface of the supporting substrates. For instance, in the case of COF-5,[30] the traditional synthesis route is as follow: the polymerization of 2, 3, 6, 7, 10, 11-hexahydroxytriphenylene (HTTP, 1) and 1, 4-phenylenebis(boronic acid) (PBBA, 5) was conducted in a Pyrex tube with mesitylene and dioxane as solvents. The reaction mixture was heated to 100 ºC for 72 h to yield a free-flowing gray-purple powder. To deposit the COF powders on the substrate for thin film formation, the most native way might be to directly submerge the substrate into the bulk COF reaction liquid.

SLG with remarkable photoelectric properties, especially the 2D atomically precise structure, is a suitable interface for coating 2D layered materials and can be transferred to other different substrates.[67] Dichtel and co-workers demonstrated that oriented COF thin films can be formed on SLG supported by different substrates, such as SLG/Cu, SLG/SiC, SLG/SiO_2, under straightforward solvothermal conditions.[53] Specifically, the COF-5 thin films was formed under the solvothermal condensation of HHTP (1) and PBBA (5) at 90 ºC in the solution of mesitylene and dioxane with the presence of SLG/Cu substrate (Fig. 4a-c). The hexagonal lattice of the COF-5 grains aligned parallel to the substrate surface, which was verified by powder x-ray diffraction (PXRD) and grazing incidence diffraction (GID). This simple synthetic method is general for

SLG transferring to other substrates including transparent fused SiO_2 (SLG/SiO_2). Importantly, the supporting substrates exert a great impact on the qualities of the thin films containing the uniformity and thickness. In the same reaction time, thicker films were obtained on SLG/Cu compared with that of SLG/SiO_2. Subsequently, they further fabricated the HHTP-DPB COF thin films with a thickness of 132 ± 18 nm and a series of Zn phthalocyanine (ZnPc, 4) COF thin films with an average thickness of 370 ± 30 nm on the transparent SLG/SiO_2 substrate.[68, 69]

Soon after, Bein *et al.* fabricated a novel thiophene-based BDT-COF thin film containing an electron donor unit.[70] Different from Dichtel's work,[53, 68, 69] a lower concentration of starting monomers with Indium-doped tin oxide (ITO)-coated or NIO/ITO-coated glass substrates was employed. As a result, a smooth and continuous organic thin film with the thickness of 150-nm on ITO-coated glass substrate was observed from the top-view and cross-sectional scanning electron microscopy (SEM) images (Fig. 4d and e). X-ray diffraction (XRD) measurement was employed to analyze the crystallinity of the thin films. The absence of peaks at low 2θ (<20°) is related to the mesoporous structure, while the strong and sharp diffraction peak at 26.1° is referred to the π-π stacking of COF layers. And GID investigation was further utilized to reveal the preferred orientation of COF thin films that COF layers with preferential orientation to the surface of ITO-coated glass were synthesized verified by the reflection concentrated near q(z) = 0. The authors also grew BDT-COF thin films with high quality on other polycrystalline inorganic substrates including NiO/ITO-coated glass and Au substrate, which led to a conclusion that, in contrast to the previous thinking, the π-π interaction is not the necessary reason for the oriented film growth. Later, Liu and co-workers prepared another electron donor contained TTF-COF by using the conventional solvothermal method.[71] In-sur oriented growth of TTF-COF thin films on Si/SiO_2 substrate and transparent ITO-coated glass were also obtained.

While boronic ester COFs and some Schiff base COFs show poor oxidative and hydrolytic stabilities, β-ketoenamine-linked COFs are another class of COFs which exhibit excellent chemical stability to water and aqueous acid. In 2015, Dichtel *et al.* developed the β-ketoenamine-linked anthraquinone-based COF (DAAQ-TFP COF) thin films by the modified solvothermal synthesis.[72] Considering that the quick reaction rate leads to the out-of-order thin film, the triformylphluroglucinol (TFP, 17) was added slowly into the mixture of 2, 6-diaminoanthraquinone (DAAQ, 25) and Au substrate instead of directly putting the substrate in the reaction liquid. The absence of N-H stretch along with the presence of C-N stretch at 1250 cm^{-1} and C=C stretch at 1560 cm^{-1} in Fourier transform infrared spectroscopy (FT-IR) characterization verified the production of β-ketoenamine linkage. The vertically oriented, layered structure was further confirmed by GIDX with the observation of the (001) peaks at $Q_{\perp}$ = 1.8 $Å^{-1}$ and $Q_{\parallel}$ = 0. As demonstrated by the authors, the thickness upper limit of this DAAQ-TFP COF thin film was 300-400 nm in practice, which is related to the initial concentration of the reactive monomers. Then, another β-ketoenamine COF (DAB-TFP COF) thin films were successfully prepared on various metals and oxides through solvothermal strategy.[73] In a previous report,[74] DAB-TFP COF was fabricated by condensing *p*-phenylenediamine (DAB, 22) with TFP (17) in a sealed glass. As this classical reaction condition was not suitable for the homogenous COF thin film growth, Lu *et al.* modified the synthesis method by growing COF thin films on ITO substrate in an autoclave. From the top-view and cross-sectional SEM images, the as-prepared DAB-TFP COF thin film was smooth and homogeneous with a thickness of approximately 200 nm (Fig. 4f and g). XRD and GID measurements confirmed the crystallinity of the thin films. XRD pattern of the obtained thin films revealed no reflection at low 2θ degrees while a strong reflection at 27° with respect to the π-π stacking of DAB-TFP COF layers emerged. In the GID image, in-plane and out-of-plane diffraction of thin films were observed clearly conformed to the bulk DAB-TFP COF. In addition to the ITO substrate, the DAB-TFP COF thin films were able to grow on other substrates, such as silicon, fluorine doped tin oxide (FTO) and platinum.

In classical imine-linked COF fabrication, aldehyde and amine moieties would produce amorphous polyimine sediments during the solvothermal synthesis with the presence of aqueous acetic acid catalyst which hinders the nucleation and growth of COF. Very recently, Yaghi and co-workers introduced a new homogenous synthetic route to fabricate imine-linked COF.[75] In this newly developed route, tert-butyloxycarbonyl (Boc) group was employed to protect amine to avoid amorphous polyimine formation. More importantly, this method is also helpful for oriented growth of imine-linked COF thin film. As an example, LZU-1 COF thin films were obtained via immersing the substrate into the reaction system which contained 4-(tert-butoxycarbonylamino)-aniline (NBDPA, 30) to protect the amine moieties. With the homogenously formation of protonated COF crystals, the nucleation of COFs would be favored of the nucleation barrier facilitating the growth of COF thin films. The as-prepared COF thin films were highly oriented and uniform with the thickness of 190-nm which can be tailored by varying the concentration of the growth liquor and reaction time.

2.2 Interfacial synthesis

Interfacial synthesis is a widely used approach for polymer thin films fabrications such as polyamides nanofilms and graphdiyne nanosheets.[76-78] In this approach, the interface is where the reaction between monomers occurs. Thus, the COF growth is limited to the confined interface region, leading to the formation of thin films. Two kinds of interfaces have been used in COF thin films synthesis, *i.e.*, liquid/air interface and liquid/liquid interface.

Recently, Bao and co-workers developed a new synthetic method to grow COF thin films at the solution/air interface given that the interface such as liquid/air interface is beneficial to the growth of COF thin films due to the good control of COF nucleation as well as the thickness.[79] Trisamine 2,6-dicarbaldehyde-4,8-dioctyloxybenzo[1,2-b:3,4-b']dithiophene (BDTA, 18) and bisaldehyde tris(4-aminophenyl)amine (TAPA, 27) were selected as the building blocks to form polyTB COF. For the formation of polyTB thin films, a highly reflective thin film

was first obtained by two days reaction of BDTA and TAPA in a covered petri dish at the solution/air interface. However, the prepared COF thin films were too rough to be incorporated into devices. To get COF films with smooth surface, the authors improved the method by using diluted mother solution filtered from bulk polyTB synthesis as the film growing solution at the solution/air interface. The thickness control could be achieved by varying the incubation times. In this work, the thinnest and thickest films were 1.8 nm and 29 nm, respectively, and both had a roughness of 0.2 nm on average. More recently, Zhang and co-workers prepared a monolayer imine-linked COF at the water/air interface by using dynamic imine chemistry.[80] Terephthalaldehyde (13) and 1, 3, 5-trihexyl-2, 4, 6-tris(4-aminophenyl)benzene (33) were selected as monomers. Three hydrophobic n-hexyl groups of the monomer 33 would set upright on the surface and extend to the air, while the phenyl rings might be fixed by the hydrophilic amino groups at the water/air interface, which made monomer 33 ideal for the interfacial reaction. Moreover, reversible imine linkage would induce self-correction and therefore lead to few defects. In this typical experiment, a dilute mixture of monomers in chloroform was spread on the water/air interface and run overnight. A smooth, free-standing monolayer sheet was then obtained with a thickness of 0.7 nm under the well-designed control.

For the liquid/liquid interfacial polymerization, two non-miscible liquids are utilized to create the interface at the junction. For example, Dey *et al.* successfully synthesized a series of large-scale thin films at the interface of water/dichloromethane.[81] To take an example, Tp (17) was dissolved in dichloromethane, and 2, 2'-bipyridine-5, 5'-diamine (Bpy, 42)-*p*-toluene sulfonic acid (PTSA) salt was added into water on the top layer. The reaction took 72 h at room temperature to obtain free-standing Tp-Bpy thin films with highly crystalline nature. The thickness of the thin films is well adjusted by the selection of the precursor concentrations. And the thin films could be easily transferred to arbitrary substrates, such as metallic wires, holey grids and glass surfaces, and in the meantime, remained the integrity of the crystalline structure and physical shape. In another report, an imine-linked TAPB-PDA COF thin film was presented at the liquid/liquid interface by the polymerization of terephthalaldehyde (PDA, 13) and 1, 3, 5-tris(4-aminophenyl)benzene (TAPB, 26).[82] Different from traditional interfacial reaction, $Sc(OTf)_3$ was employed to facilitate the imine formation and limit the polymerization at the interface. The Lewis acid catalyst $Sc(OTf)_3$ with water tolerance shows better solubility in the water phase compared with that in the organic phase. As a result, $Sc(OTf)_3$ catalyst are preferentially dissolvable in the water phase while COF monomers with preferred organic solubility were transferred to the organic phase. This spatial segregation of COF monomers and catalyst enabled the site-selective polymerization to provide a thin film at the organic/water interface. Specifically, water was added to the mixture solution of PDA, TAPB and 1, 4-dioxane/mesitylene which contained small amounts of $Sc(OTf)_3$ (Fig. 5a). The lateral dimension of the as-prepared thin films was greatly depended on the size of the reaction vessel. And the thickness of COF thin films could be easily adjusted by varying the original monomer concentration and/or the volume of the organic phase. Importantly, the thin films were readily transferable to various substrates and the integrity retained, even if it was the thinnest film.

2.3 Room temperature vapor-assisted conversion

Considering the instability of fragile building blocks which are sensitive to the harsh conditions used in solvothermal synthesis, Bein and co-workers came up with a mild method named room temperature vapor-assisted conversion synthesis.[83] Benzodithiophene-based BDT-COF and COF-5 were employed to verify this strategy. Taking BDT-COF as an example, a mixture of benzodithiophene diboronic acid (BDTBA, 8), HHTP (1), dry acetone and absolute EtOH was first filtered through a syringe filter after ultrasonication. Then, the obtained BDTBA/HHTP mixture was drop-casting on a glass substrate, followed by putting the substrate into a desiccator together with a small glass vessel loaded with mesitylene and dioxane. A dark-green organic layer with the thickness of 7.5 μm can be obtained after 72 h at room temperature. It should be noted here that the thickness control can be achieved by tailoring the droplet volume as well as the concentration. Specifically, when decreasing the droplet volume to 2/5 of former used volume and keeping other conditions the same, the thickness of the COF thin films can be reduced to 2 μm. On this basis, changing the concentration of the droplet to 1/3 of the previous concentration, a homogeneous BDT-COF films with the thickness of 300 nm was obtained. This excellent method allows constructing COF thin films with fragile precursors as well as on sensitive substrates, and therefore leads to wider applications.

2.4 Synthesis under continuous flow conditions

In contrast to the conventional static growth procedure, Dichtel *et al.* synthesized a smooth and dense COF thin film under continuous flow conditions recently.[84] Considering the poor control over the polymerization in previous method, they modified the 2D COF thin films growth using a flow cell, which enabled the COF formation amenable. In order to synthesize COF-5 in a flow cell, the monomers HHTP (1) and PBBA (5) first reacted slowly at 25 ºC, and then COF-5 formed after 2 min of induction period when the temperature rose to 90 ºC. Specifically, the reaction mixture was pumped through a reservoir with a heated temperature of 90 ºC, and then entered into a flow cell equipped with a quartz crystal microbalance (QCM) substrate for mass deposition monitor. The authors investigated the relation between the reaction conditions (temperature, resident time, reaction mixture composition, and the flow rate) and thin film formation. For example, the resident time changes the average polymerization degree of reaction mixture when it reaches the substrate. Specifically, short resident time results in monomers and small oligomers encountering the QCM substrate, while longer resident time makes for larger species reaching the growth substrate. Meanwhile, a series of boronate ester-linked COFs, DPB-COF, TP-COF, and COF-10 were grown in flow to confirm the suitability of the method. As a result, for the first time, constant deposition rate can be achieved and film thickness can be controlled under continuous flow conditions.

The COF thin films fabricated via bottom-up strategy are summarized in Table 1. As mentioned previously, while there are several methods with respect to bottom-up strategy, the simple and straightforward solvothermal synthesis is the most frequently used method. However, limitations still exist: (1) unreacted monomers and small oligomers may contaminate the thin films and block the pores; and (2) it is difficult to monitor the nucleation during the film formation. Synthesis under continuous flow conditions solves the problem of thin film contamination, however, in the cost of monomer waste. The approach related to the reuse of unreacted monomers needs to be explored. In that case, room temperature vapor-assisted conversion synthesis and interfacial synthesis seem to be more attractive, but their applicability requires the further research. In short, more comprehensive studies about optimal reaction conditions such as temperature, concentration and reaction times of COF thin film growth are clearly warranted, and the influence of the chosen substrate should be discussed deeper. Moreover, additional methods are still needed.

3. Top-down strategy for the fabrication of COF thin films

Different from the abovementioned bottom-up strategy, the top-down method means simple preparation of free-standing single-/few-layered COF thin films from bulk materials, instead of growing it on specified substrates or interface. Compared to the bottom-up method that is usually expensive and needs strict conditions, the top-down method is cheaper and more straightforward. As we know that bulk 2D COF crystals are layered structures with different layers stacked each layer along the vertical direction via weak interactions including van der Waals force and/or hydrogen bonding. The top-down synthesis is designed to break the π-π interactions between the COF layers by internal or external force to produce single or few-layered free-standing COF thin films. In this section, we will demonstrate various synthetic methods in regard to top-down strategy including solvent-assisted exfoliation, mechanical delamination, chemical exfoliation and self-exfoliation. The distinction between these different ways comes from the source of the peel strength. For example, the self-exfoliation method mainly relies on the internal force while the solvent-assisted exfoliation and mechanical delamination are caused by external force. In the following, all the different methods will be elaborated separately.

3.1 Solvent-assisted exfoliation

As the most commonly used method for COF exfoliation, a plenty of examples could be found in the published works.[59, 85-88] This review selects several representative cases to elucidate this simple but effective method. Inspired by the successful exfoliation of graphene by sonication in well-chosen solvents,[89] Berlanga *et al.*, for the first time, obtained the delaminated CONs with 10-25 layers by using solvent-assisted exfoliation method.[59] Boronic ester-linked COF-8 was selected as the bulk sample, which was synthesized by the condensation of HHTP (1) and BTPB (9) demonstrated in previous literature.[90] The authors expected to weaken the π-π interactions between COF layers via mechanical force like sonication with the help of suitable solvent. This is possible given that sonication can accelerate the intercalation of solvent molecules into the COF, which increases the interlayer space and therefore weakens its interlayer interaction. Moreover, solvent plays an important role in the exfoliation of the layered COFs, which not only exfoliates the layered COFs but also stabilizes the as-formed nanosheets. Specifically, suitable surface tension between the layer crystal and solvent is a key point in lowering the energy and improving the efficiency of exfoliation. Particular solvent with COF-matched surface energy enables the balance of the exfoliated energy.[89, 91] Low exfoliation rates are found when an improper solvent is used. Furthermore, proper solvent can also prohibit the aggregation of the nanosheets.[92] Among the solvents utilized, CH_2Cl_2 stood out because of its excellent properties such as suitable surface energy, volatility and high chemical purity. A certain amount of COF-8 powders was dissolved in anhydrous CH_2Cl_2 and the mix liquor was sonicated for 15 min. The consequent suspension was then centrifuged for 5 min leading to a color-less solution. Finally, the solid residue of the solution was characterized by infrared radiation (IR), X-ray photoelectron spectroscopy (XPS), and so on. Specifically, the IR signature of the delaminated CONs was same as that of COF-8 bulk powders. As revealed by the XPS data, the exfoliated CONs showed different graphic feature which indicates a disruption of the interlayer interactions and the obtainment of randomly oriented sheets. The as-prepared sheet-like structure was further confirmed by AFM and TEM. It is worth mentioning that the obtained CONs could be transformed to any substrates without affecting the original properties. To better understand the influence factors with respect to the COF exfoliation, a further research on the effects of COF structure on the exfoliation was introduced.[85] A series of poly(aryleneethynylene) COFs with different pore size (from 1.4 to 3.3 nm) was employed to study the impacts of porosity and reaction time. This kind of COFs was constructed by carbon-carbon bonds via Sonogashira-Hagihara coupling procedures.[93] The results showed that smaller pore size and longer sonication time lead to thinner CONs which means higher degrees of exfoliation. Importantly, the impact of porosity can be weakened by the increase of sonication time.

However, the application of the as-synthesized boronate ester COF thin films is limited due to its poor hydrolytic and oxidative stability as well as the palpable interlayer stacking energies. As the acyl hydrazones could overcome the above drawbacks, Dichtel and co-workers prepared the 2D hydrazone-linked COF-43 thin films under mild conditions and further proved the feasibility of the solvent-assisted exfoliation method (Fig. 6a).[86] COF-43 was fabricated by the method reported previously and confirmed by PXRD.[36] Interestingly, the crystallinity of COF-43 became weak when the powder was submerged into the dioxane, H_2O, and DMF which was different from that of other common solvents such as THF, $CHCl_3$ and MeOH. In order to prove that the weakness of crystalline was resulted from the exfoliation of the multilayers rather than the disruption of covalent bond, the authors first eliminated the hydrolysis process proved by FT-IR and solid-state IR which demonstrated the integrity of hydrazine links. Then, AFM and

selected area electron diffraction (SAED) data of the contrast experiment further verified the exfoliation of layered COF-43 and the function of solvent in the case of COF-43 exfoliation that exfoliating solvents led to thinner COF-43 nonasheets while non-exfoliating solvents obtained poor-constructed COF-43 multilayers. Very recently, another imine-linked TPA-COF thin films were prepared by Zhang and co-workers via simply sonicating TPA-COF-ethanol mixture.[87] TPA-COF powders were dispersed in ethanol and the mixture was then sonicated for 3 h. After 24 h stewing, the upper colloidal suspension containing exfoliated TPA-COF nanosheets was collected and centrifuged. The free-standing TPA-COF thin films were left as sediments. TEM characterization confirmed the 2D nanosheets structure and AFM image showed that the thickness of as-synthesize TPA-COF thin film was 3.5 ± 0.3 nm equivalently to 9 ± 1 layers (Fig. 7a and b). Interestingly, this ultrathin quality enabled the visualization of detailed structure information of TPA-COF nanosheets such as pore channels and building units via low-dose imaging technique of TEM for the first time (Fig. 7c and d).

3.2 Mechanical delamination

Another effective and precaution-free method, namely mechanical delamination, was employed by Banerjee *et al*.[94] When fabricating TpPa-1 and TpPa-2 by using a solvent-free room-temperature mechanochemical method, it was discovered that the exfoliated COF layers also existed.[95] As demonstrated by the authors, mechanical grinding would break the strong π-π interactions between COF layers which made the COF exfoliation possible. With this in mind, they further prepared a series of TpPa and TpBD COF thin layers under the same condition (Fig. 5b). A certain amount of bulk COF materials was put in a mortar with several drops of methanol and then fully grinded by a pestle at room temperature for 30 min. Then, the collected powder was dispersed in the methanol solution and centrifuged until a clear liquid was obtained. The free-standing COF thin films were obtained after completely evaporating the solvents. The TEM image and AFM measurement confirmed the existence of flat nanosheet-like structures with the thickness of ~10 nm corresponding to ~10-30 COF layers (Fig. 7e and f). Meanwhile, the FT-IR and Raman spectroscopies indicated the structure integrity of COF thin films after delamination except for the decrease of crystallinity which was verified by the PXRD profile. Moreover, these COF thin films remained stable in both acidic and basic solutions similar to their parent COFs.

Different from the mortar & pestle system, another scalable and simple mechanical delamination method with respect to ball milling was employed to delaminate an anthraquinone based COF (DAAQ-TFP-COF).[96] The vibratory ball worked at room temperature with the DAAQ-TFP-COF materials put in a milling pot without any other exfoliating agents to obtain DAAQ-TFP-COF nanosheets. Thickness was tailored by changing the vibration frequency and time. By elegantly selecting the vibration frequency of 50 Hz for 0.5 h, a free-standing DAAQ-TFP-COF thin film with a thickness of 3-5 nm was obtained. Later on, Hu and co-workers also fabricated the melamine/*o*-phthalaldehyde condensed CONs using modified ball milling method.[97] The COF was prepared via solvothermal procedure.[98] Then the as-prepared COF was wet-ball milled in the presence of DMF at 225 rpm for 24 h and sonicated 30 min for dispersion. The obtained mixture was centrifuged to collect supernatant which was regarded as CONs. Comparing the XRD patterns of bulk COF and the given CONs, the intensity of the characteristic diffraction peak at around 23.5° dropped remarkably related to CONs indicating the production of CONs considering the crystalline damage caused by the external ball milling force. On the other hand, the COF and CONs shared similar chemical structure despite the slight change as evidenced by the FT-IR spectrum. TEM image verified the multihole nanosheets. XPS spectra was employed to investigate the bond state and atom composition of the samples. The characteristic peaks of C_{1s} in high-resolution XPS spectra were assigned to C−C (284.7 eV), C−N (285.4 eV), C=N (287.4 eV), and C=O (280.0 eV). Two typical peaks were revealed in N_{1s} high-resolution XPS spectra, comprising N=C (389.5 eV) and N−H (399.9 eV). And the atomic percentage of carbon, nitrogen, and oxygen was 64.86%, 27.57%, and 7.62%, respectively. As a result, the CONs were successfully exfoliated from COF counterparts by ball milling.

3.3 Chemical exfoliation

Considering the poor dispersion stability and the difficult thickness control of exfoliated CONs,[35, 99, 100] Khayum *et al*. synthesized the N-hexylmaleimide-functionalized CONs chemically exfoliated from an anthracene-based COF by [4 + 2] cycloaddition reaction (Fig. 8a and b).[101] And a centimeter-scale self-standing COF thin film was further obtained at water/air interface via layer by layer assembly. As known, 9- and 10-position of anthracene units are easy to be attacked via [4 + 2] cyaloaddition reaction.[102] The π-π stacking between layers and the planarity of each layer can be weakened with the intercalation of N-hexylmaleimide into the COF backbone which leads to the COF exfoliation. In this exfoliation process, the anthracene-based imine-linked COF DaTp was first condensed by 2, 6-diaminoanthracene (Da, 24) and Tp (17) through standard solvothermal protocol. Then [4 + 2] cycloaddition reaction was employed to introduce N-hexylmaleimide into DaTp, which led to the weaker π-π interactions between COF layers, and thereby obtained the exfoliated DaTp COF nanosheets. Considering that the long alkyl chains and dipole forces can make it possible for DaTp COF nanosheets to form thicker thin films by layer by layer assembly, a conventional air/water interfacial layer by layer assembly method was employed to control the thickness.[103] A suspension of DaTp COF nanosheets in dichloromethane (DCM) was added drop wise into a beaker of water, where water served as the liquid phase considering the fact that the hydrophobic alkyl chains enable the levitation of the nanosheets on the surface of water, while DCM with lower surface energy and higher vapor pressure was act as the spreading solvent. A temporary DCM-water bilayer was generated by quickly spreading the nanosheets suspension to the water surface, and a semi-transparent COF thin film was obtained after rapidly evaporating the DCM layer within 60 seconds. SEM, AFM and optical microscopy images further

indicated the formation of a continuous, defect-free, and free-standing COF thin film with a thickness of 5-6 nm (Fig. 8c-f). To verify the thickness control of layer by layer assembly, three parallel experiments with different suspensions were also conducted, which indicated that higher concentration led to thicker films.

Later, the same group further expanded the research to synthesize CONs via post-synthetic modifications.[5] Hydroxyl (-OH) units are perfect moiety for modification because of their facile derivatizable nature under moderate conditions.[104] Keeping this in mind, the authors elaborately chose 4-aminosalicylhydrazide (ASH, 36) as one of the linkers for COF construction while 4-aminobenzohydrazide (APH, 34) without hydroxyl was chosen for comparison. 1, 3, 5-triformylphloroglucinol (Tp, 17) and diamines (APH, 34, or ASH, 36) were condensed with the existence of PTSA through a neoteric solid-state mixing procedure to synthesize TpAPH and TpASH. And a three-step approach was employed to obtain functional target CONs. First, with the adding of glycidol (Glc), the phenolic hydroxyl groups were converted to alkyl hydroxyl groups to make TpASH-Glc CONs by opening the epoxy ring. Then the as-synthesized surface alkyl hydroxyl groups were transformed to amines in the presence of APTES for amine functionalized CONs producing. Finally, the cellular targeting ligand folic acid (FA) was involved to fabricate objective CONs (TpASH-FA). As demonstrated by the authors, the as-prepared CONs owned excellent aqueous dispersibility due to their surface functionalization.

3.4 Self-exfoliation method

In contrast to developing CONs with the aid of the external force, the self-exfoliation method is more likely to depend on the well-designed building block to induce the peeling-off by internal force. For example, in El-Kaderi *et al.*'s work,[106] the π-π interactions between the as-prepared COF layers were reduced due to the insert of triptycene units. Based on this, two methyl groups were introduced into the 9, 10-position of triptycene tricatechol (TPTC, 2) to further enlarge the distance between the COF layers, which enabled the exfoliation of monolayer COF thin film.[106] More recently, Rahul Banerjee and co-workers incorporated guanidinium units into the COF backbone to obtain self-exfoliated ionic covalent organic thin films.[107] The authors fabricated three different CONs ($TpTG_{Cl}$ (Fig. 9a–b), $TpTG_{Br}$, and $TpTG_{I}$) through Schiff-based condensation using the conventional solvothermal synthesis. From the PXRD pattern, the crystallinity of the obtained CONs was relatively low. Weak π-π stacking between the layers could be verified by the broad peak at 2θ = ~27.3°. On the other hand, with the molecular dynamics (MD) simulation studies, the average interlayer π-π stacking distance of $TpTG_{Cl}$ was increased from initial 3.338 Å to ~5.5-6 Å. The authors ascribed this to the inherent positive charge of guanidinium units and the existence of the loosely bound chloride ions, and concluded that the ionic CONs with 3-6 layers were successfully synthesized, which was further proved by TEM analysis as well as AFM measurements (Fig. 9c–h).[106, 108] Compared to other breaking-off methods, self-exfoliation method seems to be a simpler way because of its internal synthesis and avoided restacking. Moreover, it's possible to use ionic building units not only to start up the self-exfoliated process but also act as targeted functional group, which broadens the applications of COF thin films.

The free-standing COF thin films fabricated via top-down strategy are summarized in Table 2. Four major fabrication methods related to top-down strategies have been explored. Obviously, solvent-assisted exfoliation is the most frequently used method. Compared with other methods, this method enables the high-yield and massive production of ultrathin nanosheets in solution at low cost, since the process is quite simple. Chemical exfoliation and self-exfoliated process are able to introduce functional groups not only avoiding aggregation but also acting as targeted function. As for solvent-free mechanical delamination, toxic organic solvents are well avoided. While the aforementioned methods have their respective advantages and have succeeded in the preparation of free-standing COF thin films, there still have some shortages. On the one hand, the obtainment of true single-layered nanosheet is difficult and the aggregation of monolayers exists because of the stacking interaction; on the other hand, the yield of CONs is relatively low, which hinders the industrial applications. What's more, the generality of the methods has to be proven. What is worth mentioning is that colloidal suspensions of COFs provide new opportunities for free-standing COF thin films.[109, 110] Solution-casting of COF colloids enables to obtain free-standing films with controlled size and thickness. For example, Dichtel *et al.* reported a COF-5 film formed by evaporating solvent from a colloidal suspension.[109] The as-prepared film retains the integrity of crystallinity same as the original colloidal solution and exhibits a preferential orientation compared with that of thin films obtained from in-suit growth on the substrates. These results represent an important aspect for the developing free-standing COF thin film using top-down strategy and further studies are also needed to decode the film aggregation mechanism.

4. Applications of COF thin films

The application of bulk COFs suffers a lot from their insoluble and unprocessable characters. It is necessary to facile synthesize long-range ordered COF thin films for better performance. As demonstrated above, various synthetic methods have been employed in the COF thin films fabrication. One can understand that different synthetic methods lead to different properties of materials and therefore the different applications. In this section, we will discuss the existing works that COF thin films have been employed to achieve specialized functions and summarize the applications covering energy storage, separation membranes, chemical sensors, *etc*.

4.1 Energy storage

With the population growth and industrial explosion, one of the most serious problems facing the world is energy shortage. Clean, renewable energy sources and energy storage devices including lithium ion battery, supercapacitors, and solar cells are urgently needed.[111-113] COF thin films with enhanced

specific area, ultrathin thickness and accessible functional sites are considered as promising platform for energy storage applications. Some intriguing progress have been made in energy storage based on COF thin films in recent years.

4.1.1 Lithium-ion batteries. Theoretically, ultrathin COF thin films with limited layers enable the reduction of ion/electron migration length as well as the facilitation of ion/electronic diffusion. Moreover, a mass of available Li sites on or near the surface also endow the rapid charge-discharge cycles and the full utilization of redox sites. Anthraquinone as a redox-active unit has attracted considerable attention in the application of energy storage.[114-116] Wang *et al.* conducted a research on the usage of free-standing anthraquinone-based COF thin films in Li^+ batteries. Compared with bulk COF powders, the exfoliated COF thin films owned the enhanced efficiency of redox-active sites utilization and the rapid kinetics for lithium storage due to their shorter Li^+ diffusion pathways. In a typical experiment, a redox-active DAAQ-ECOF with the thickness of 5 nm was prepared via mechanical milling method. In the process of charge-discharge cycles at 20 mA g^{-1}, DAAQ-ECOF delivered 96 % (145 mA h g^{-1}) of its theoretical capacity after 70 cycles, while only 73% have been achieved by its pristine counterpart DAAQ-TFP-COF. After 1800 cycles of charge/discharge, DAAQ-ECOF still possessed a reversible capacity of 107 mA h g^{-1} at 500 mA g^{-1} and 98% capacity retention. Interestingly, with carefully molecular design, the capacity could be improved to 210 mA h g^{-1} and the discharge voltage could be increased to 3.6 V. In another study, Chen *et al.* explored the Li^+ conductivity of CONs, which is important for the construction of Lithium batteries. The target product Li-CON-TFSI was synthesized via a three-step method. Briefly, they first synthesized the cationic CON with chloride counterions (CON-Cl) by self-exfoliation method. Then, intermediate CON-TFSI was formed through an ion exchange between CON-Cl and lithium bis(trifluoromethane) sulfonimide (LiTFSI). Li-CON-TFSI was finally obtained after drying the mix of LiTFSI salt and CON-TFSI which was dissolved in ethyl alcohol liquor. The as-prepared Li-CON-TFSI showed a significant increased conductivity of 2.09 × 10^{-4} S cm^{-1} at 70 °C which was higher than that of MOF/COF based electrolytes with plasticizers.

4.1.2 Capacitors. As known, Anthraquinone-based materials are also frequently used as organic redox couples for electrochemical capacitors,[117, 118] whereas the electroactivity of anthraquinone is relatively low leading to a bad cycle stability.[119, 120] Zha *et al.* developed a kind of anthraquinone-contained COF thin films on 3D graphene ($COF_{DAAQ-BTA}$-3DG) as a promising negative electrode for hybrid electrochemical capacitors.[121] Layered $COF_{DAAQ-BTA}$-3DG enabled the increased mass loading of anthraquinone and an improved accessibility of anthraquinone moieties up to 13.45% in an alkaline media. The capacitance of as-prepared $COF_{DAAQ-BTA}$-3DG was 31.7 mF cm^{-2} which can be well-used as capacitive electrode in alkaline condition. Later, Dichtel and co-workers also synthesized an anthraquinone-based DAAQ-TFP COF thin film on Au substrate.[72] Cyclic voltammetry experiments confirmed that a larger percentage of anthraquinone in DAAQ-TFP COF thin films was electroactive compared with that of COF powders.[38] Though poor proton transfer in thin-film electrode led to slow charge transfer, a much large proportion of accessible anthraquinone subunits enabled the increased conductivity through electron self-exchange process. Furthermore, as demonstrated by Galvanostatic Charge Discharge Cycles (GCDC) experiments, the charge storage capabilities increased by 7.5 times with the utilization of DAAQ-TFP COF thin films. The results revealed that the DAAQ-TFP COF thin films have great potential to be incorporated into supercapacitors.

4.1.3 Solar cell and fuel cell. Early in 2011, Dichtel and co-workers pointed out that the high crystallinity and orientation of COF thin films on SLG/SiO_2 substrates have the potential to construct photovoltaic devices with designed functional π-electron systems and pioneered the research by growing crystal and aligned tripenylene-pyrene COF thin films and phthalocyanine COF thin films on SLG/SiO_2 surface for further photovoltaic applications.[53] TP-COF was synthesized by the polymerization of HHTP (1) and Pyrene-2, 7-diboronic acid (PDBA, 6), while NiPc-PBBA COF was condensed by Ni octahydroxyphthalocyanine (NiPc, 3) and PBBA (5). The GID dates of TP-COF thin films and NiPc-PBBA COF thin films revealed the vertical alignment of the 2D lattice. The photoluminescence of TP-COF thin films showed the characteristic peak of pyrene excimer emission over all excitation wavelengths indicating the efficient energy transfer from HHTP to pyrene. For NiPc-PBBA COF thin films, the adsorption bands in the visible region of the spectrum derived from Ni phthalocyanine chromophores. Both TP-COF thin films and NiPc-PBBA COF thin films are ideal precursors for photovoltaic applications. Besides, Montoro *et al.* demonstrated the potential of COF thin films for fuel cells.[122] RT-COF-1Ac and RT-COF-1AcB were prepared based on the condensation of TAPB (26) and 1, 3, 5-benzenetricarbaldehyde (BTA, 14). And a post-synthetic strategy was employed to obtain LiCl@RT-COF-1 from the reaction between RT-COF-1 and LiCl. The films of RT-COF-1Ac, RT-COF-1AcB, and LiCl@RT-COF-1 were selected to test their performance to act as solid electrolytes in proton-exchange membrane fuel cells (PEMFCs) (Fig. 10). Characterized by a series of measurements, the RT-COF-1AcB films displayed the best performance. For RT-COF-1AcB film-based PEMFCs, an optical balance between high conductivity values and low H_2 fuel crossover under 1.1× 10^{-2} S cm^{-1} at 323 K led to the maximum current density (53.1 mA cm^{-2}) and maximum power density peak (12.95 mW cm^{-2}).

4.2 Semiconductor devices

The structural features of COFs are advantageous for carrier transportation in semiconductor electronic devices. Lots of researches on fabricating functional electron units into 2D layered COFs to construct electronic devices with high performance have been reported.[123, 124] Despite the promising results, it is hard to incorporate bulk COFs into devices with full contact, which leads to the weak performance because of the insolubility of COF powders. In addition, the low intrinsic conductivity also hinders their applications.[125] Single or few layered COF thin films offer considerable potentials for the fabrication of semiconductor device. The unique properties of

the electronic COF thin films enable them to be used as semiconductor devices with high performance.

Tetrathiafulvalene (TTF) building block has been used as electroactive unit to synthesize semiconducting COFs.[126, 127] While the charge-carrier mobility in bulk COF is high, the COF powder nature weakens their applications. Cai *et al.* reported an oriented TTF-COF thin films and its doping related conductivity.[71] The porous nature of TTF-COF thin films enables the infiltration of electron acceptors such as I_2 or tetracyanoquinodimethane (TCNQ) as charge-transfer partners.[128] The authors fabricated TTF-COF thin films with Au/Cr electrodes to detect the conductivity. Comparing the *I-V* curves of the TTF-COF thin film device before and after exposure to I_2, electronical conductivity of the device significantly increased with the existence of I_2 vapor. In the 24 h-exposure, the conductivity increased to a maximum of 0.28 S m^{-1} which was three times order magnitude higher than that of the pristine film and among the highest for COF materials. While being removed from the I_2 vapor, the conductivity of the device decreased to 1.0 ×10^{-3} S m^{-1}. The authors also used TCNQ as a non-volatile dopant to further verify the doping influence. Similar to the I_2 doping, the conductivity increased after immersing to a solution with TCNQ, and then remained stable even after removing the TTF-COF thin films from the solution. In addition, PXRD analysis was performed to verify the retained crystallinity of the TTF-COF after doping. As electronical transport properties significantly depend on the film morphology and molecular arrangement,[129-131] Medina *et al.* investigated the directed charge carrier transport as well as the additional electrical properties using oriented BDT-COF thin film device as a model system.[132] The charge-carrier transport along the columnar stacks is an important factor for judging the overall performance of COF thin films based devices. An oriented BDT-COF thin film was grown on glass-coated ITO electrode as method mentioned above. And MoO$_3$ and Au were utilized as top electrodes. Comparing the performance of the BDT-COF thin film with the thickness of 80-200 nm came to a conclusion that the thinner COF-film leads to higher hole mobilities. As demonstrated by the authors, the thickness dependence came from the inherent electron-defects in the BDT-COF stacks. Thicker films mean more layers and therefore more electronic defect in the stack. The defects cannot be efficiently evaded given that the charges cannot transport along the alternative paths. The average hole mobility tripled under illumination compared with that in the dark due to the increased charge density allowing the electronic trap states to be filled. Further, hole-only devices (HODs) was constructed to measure the columnar hole mobility in a diode configuration. Borate ester linking groups within the BDT-COF thin films enabled the high resistivity towards charge migration. The characterization of BDT-COF thin films revealed the potential of BDT-COF thin film to be a semiconductor device material.

Field-effect transistors (FETs) are organic-based electronic devices that can be used for the detection of charge transport efficiency in organic materials.[133] In-plane charge transport as well as transport in a few molecular layers challenge the FETs performance.[134] Bao and co-workers synthesized an imine-based COF (named "polyTB") film at the solution/air interface and incorporated it into a thin-film FET as a semiconductor active layer.[79] However, the average mobility of the transistors was relatively low because of the thin film defects. Later, Wang and co-workers prepared another imine-linked $COF_{TFPy\text{-}PPDA}$ thin films on SLG by solvothermal synthesis for the fabrication of Vertical field-effect transistor (VFET) device (Fig. 11a).[132, 135] VFET is an efficient electronic device constructed by drain electrode vertically stacking source electrode and channel layer.[136] The thickness of the deposited semiconducting substrate has a great influence on the short channel length. In this report, the SLG/COF-VFET device was constructed by incorporating $COF_{TFPy\text{-}PPDA}$ thin films with an average thickness of 50 nm as the transport channel while the SLG acted as the source electrode (Fig. 11b). Due to the synergistic effect of the heterostructure of $COF_{TFPy\text{-}PPDA}$ thin film and conductivity of SLG, a remarkable ambipolar charge transport behaviour of the as-prepared SLG/COF-VFET device was observed under the adjustment of supplied voltages, which may originally come from the lower injection barriers for electrons and holes injection as well as the tuneable work function and density of state of SLG (Fig. 11c-e). The narrow band gap (1.61 eV) of $COF_{TFPy\text{-}PPDA}$ can also be ascribed to the lower injection barrier for both charge carriers transporting. High $J_{on/off}$ ratio of 10^5 in *n*-type regime and 10^6 in *p*-type regime was obtained under the condition of low manipulating voltages. The highest on-current density could achieve 6.8 A cm^{-2} for hole transporting and 4.1 A cm^{-2} for electron delivering. $COF_{TFPy\text{-}PPDA}$ thin films with the remarkable ambipolar behaviour and the excellent semiconducting performance demonstrated its prospective application in semiconductor devices.

4.2 Membrane-separation

Molecular separations, especially gas separation and water purification, have aroused much attention for decades due to their importance to the development of clean energy and environmental protection.[137-140] Among the known separation strategies, membrane-based separation with the advantages of easy to design, low energy consumption and environmental friendliness is given preference.[141-143] Among the traditional membranes, employing graphene-based materials with artificially drilling holes as porous fillers exhibits moderate performance because of the structure defect or poor compatibilities.[144] While inherit porous materials such as zeolites,[145] MOFs[146-148] and zeolitic imidazolate frameworks (ZIFs)[149] show a significant potential for membrane separation owing to their ordered pore channels, these material-based membranes, which are usually prepared within polymeric matrixes or by growing them on a support, show lower performance of permeance and separation due to the covering effect within the hybrid matrixes and poor adhesion or improper growth on the support.[150-152] COF thin films with ultrathin layers, large area, tunable pore size and chemical functionality are beneficial to membrane fabrication. And membranes based on COF thin films are expected to exhibit both high permeability and high selectivity.

Recently, COF thin films have been widely used in the fabrication of nanofiltration (NF) membranes especially "thin film composite" (TFC) membranes. Kandambeth *et al.* prepared two kinds of COF membranes (COMs) M-TpBD and M-TpTD to explore their applications in wastewater treatment and organic solvent recovery.[153] The COMs with continuous surface were prepared by an optimized sequential reagent addition approach. In brief, aromatic diamine, PTSA and H_2O were firstly mixed to get an organic salt. Then the mixture and Tp (17) were shaken completely using a vortex shaker to form the dough. Knife-casting and baking were further used to make the COMs which can be exfoliated from the glass surface. The M-TpBD membranes rejection for rose Bengal (RB) was 99% while that of the M-TpTD membrane was 84% due to the smaller pore size. Moreover, as illustrated in Fig. 12, M-TpBD had a selectivity of nitroaniline over RB indicating that dye molecules with the molecular dimension above 1 nm could be rejected by M-TpBD. The COMs also showed high performance of organic solvent permeance. The acetonitrile permeance capability of M-TpTD was 2.5 orders of magnitude higher compared with that of previous reported polyamide-based nanofiltration membranes.[154] Later, the same group synthesized another series of COF thin films (Tp-Bpy and Tp-Azo) with the thickness of ~50-200 nm through interfacial process at room-temperature without knife-casting or baking.[81] The as-prepared free-standing COF thin films can be used as molecular sieve analogue to separate organic solvent. Tp-Bpy and Tp-Azo were selected to incorporate with macroporous polyester-3329 supports, respectively. Both COF thin films exhibited high solvent-permeance and solution-rejection performance. Importantly, Tp-Bpy thin films performed brilliant aceetonitrile permeance up to 339 L m^{-2} h^{-1} bar^{-1}. More recently, Matsumoto *et al.* reported a kind of poly(ether sulfone) (PES)-supported NF membranes integrated with COF thin films for the rejection of Rhodamine WT (R-WT).[82] The COF-PES membranes displayed higher R-WT rejection of 91% compared with that of PES alone. Then the same group incorporated another TAPB-PDA COF active layer into PES NF membrane to form asymmetric membranes.[155] The TAPB-PDA COF-PES membranes exhibited higher R-WT rejection and lower water permeability compared with that of PES support alone. In another report, Fan *et al.* prepared COF-LZU1 membranes on alumina tubes via solvothermal synthesis.[156] The membranes owned a remarkable water permeance up to 760 L m^{-2} h^{-1} bar^{-1} and an excellent rejection rates above 90% for water-soluble dyes with molecular dimensions larger than 1.2 nm.

Besides, COF thin film membranes can also be used in gas separation. A recent computational study reported by Zhong and co-workers exhibited the remarkable performance of ultrathin COF membranes comprised with the few stacked layered COF nanosheets. The CO_2 permeation flux was high and the CO_2/N_2 separation selectivity varied from non-selectivity to high selectivity largely depending on the stacking model.[157] Recently, Li *et al.* introduced a novel high-quality COF-1 membrane via assembling exfoliated COF-1 nanosheets on the surface of porous ceramic support.[88] Single-gas permeation of COF-1 membranes showcased a Knudsen-diffusion mechanism. The as-synthesized COF-1 membranes had a higher H_2 permeance than MOF membranes and grapheme sheets.[158-160] Moreover, the permeation performance of COF-1 membrane maintained instant under high temperature which was also better than MOF membranes.[161]

In addition to the COF thin films used as TFC membrane forms, COF thin film-based mixed-matrix membranes (MMMs) constructed by incorporating the COF layer into the polymeric matrixes have also been studied. Notably, compared to the bulk COF-based MMMs,[162-165] the enhanced stability and compatibility within polymeric matrixes resulting from the nanosheet morphology endow the MMMs with better performance. For example, Zhao *et al.* prepared two kinds of COF nanosheet-based MMMs for gas separation.[166] NUS-2 and NUS-3 nanosheets were obtained with the size of 50-100 nm via solvent-assisted exfoliation. Poly(ether imide) (Ultem) and polybenzimidazole (PBI) were selected as polymeric matrixes. The obtained nanosheets were then blended into the polymeric matrixes to produce MMMs (NUS-2@Ultem, NUS-3@Ultem, NUS-2@PBI, and NUS-3@PBI). The as-prepared MMMs showed defect-free structure with good mechanical property as a result of the superb compatibility between CON fillers and polymeric matrixes. The CON-containing MMMs exhibited higher gas permeability and/or selectivity than that of pure polymer membranes. In the case of the single gas tests, 20 wt %NUS-2@PBI exhibited a H_2/CO_2 permselectivity up to 31.4 under the condition of higher pressures which has exceeded the 2008 Robeson upper bound.[167] On the other hand, when conducting the mixed gas tests, the performance was deterioration slightly because of the competition between CO_2 and H_2 in membranes. As for water treatment, Banerjee *et al.* fabricated stable guanidinium-based CONs ($TpTG_{Cl}$) by self-exfoliation method and incorporated the as-synthesized CONs with PSF to form MMMs, namely, $TpTG_{Cl}$@PSF.[107] The $TpTG_{Cl}$@PSF has an inherent antimicrobial property by retarding bacterial growth compared to normal filler paper.[100] As this hydrophilic membranes enabling the permeation of water, this aqueous stable and antibacterial $TpTG_{Cl}$@PSF membranes are expected to be applied in water purification.

4.3 Sensors

Beyond energy storage, semiconductor device and separation membrane, sensor system is another intriguing field for the application of COF thin films.[168-170] While COFs with good photophysical properties are expected to act as efficient sensors,[171-173] the aggregation layers via π-π stacking, ineffective interaction with analytes and poor electron mobility greatly hinder the sensing ability of the bulk COF. COF thin films with high surface area, ultrathin thickness and highly accessible active sites are considered to get better performance. Early in 2011, Dichtel and co-workers synthesized HHTP-DPB COF films which have strong photoluminescent (PL) because of the cofacially packed diphenylbutadiyne moieties.[68] The vertical arranged HHTP-DPB COF films grew continuously on SLG surface with a thickness of 132 ± 18 nm, showing the potential of fluorescent sensing.

2, 4, 6-trinitrophenol (TNP), as one of the most dangerous nitroaromatic explosives, has caused some acute diseases including liver injury, headache and diarrhea, and environmental pollution.[174-176] Das *et al.* reported the utilization of TfBDH-CONs to selectively detect TNP via both turn-on and turn-off sensing mechanisms.[177] In detail, two kinds of imide-based COFs (TpBDH and TfpBDH) were synthesized by solvothermal condensation and then exfoliated to TpBDH-CONs and TfpBDH-CONs with ~ 5-15 stacked layers through solvent-assisted exfoliation. In solution phase, the PL spectra of TpBDH-CONs showed no change upon the addition of nitroaromatic analytes such as TNP, 2, 4, 6-trinitrotoluene (TNT), 2-nitrophenol (NP), 2, 6-dinitrotoluene (DNT), and 2, 6-dinitrophenol (DNP). Interestingly, TfpBDH-CONs exhibited different phenomenon that the PL emission decreased significantly with the titration of nitroaromatics (TNP, TNT, NP, DNT and DNP), and high sensitivity and selectivity of TNP were obviously observed with 63% quenching efficiency (Fig. 13a and b). In solid state, a "turn-on" sensing behaviour was found in TfpBDH-CONs-coated paper with the increase of TNP concentration (Fig. 13c and d). As demonstrated by the authors, the "turn-off" phenomenon in solution phase was caused by the electronic charge transfer between the pirate anion (TNP^-) to π-electronic cloud of the protonated TfpBDH-CONs, while the "turn-on" phonomenon in solid state was determined by the proton transfer from TNP to the basic nitrogen atom of the imine (-C=N) bond. Similarly, Zhang *et al.* prepared a fluorescent polyimide COF (PI-COF) by the condensation of tetra(4-aminophenyl) porphyrin (TAPP, 41) and perylenetracarboxylic dianhydride (PTCA, 42) and then obtained PI-CONs with a thickness of 1 nm through solvent-assisted exfoliation.[178] Benefited from the fluorescent properties along with the electron-deficient imide structure and electronic benzene ring, PI-CONs showed an excellent fluorescence quenching response to TNP with a minimum detection of 0.25 μM, and a remarkable selectivity for TNP detection over other nitroaromatics such as DNT, TNT and NP.

In addition to the chemosensors, COF thin films can also be utilized as biosensors because of their adsorption affinities. Wang *et al.* constructed an imine-linked COF thin film (Si-AMS-NH_2-4) on an amino functionalized silicon substrate (Si-AMS) by the reaction of BTA (14) and DAB (22).[179] The as-prepared COF thin films can be used as biosensor related to bovine serum albumin (BSA) adsorption and probe for DNA immobilization. In aqueous solutions, the functional units on biomolecules would undergo electrolysis, which endows them to adhere on amino-functional COF thin films through electrostatic interactions. In this report, electrochemical methods were employed to perform the biomolecule immobilization on Si-AMS-NH_2-4 and Electron impedance spectroscopy (EIS) was utilized to identify the BSA adsorption or the DNA immobilization on Si-AMS-NH_2-4 surface. As demonstrated by the authors, the electrochemical activity of Si-AMS-NH_2-4 can be strengthened when biomolecules were adsorbed onto the COF thin film, which was observed from the declined charge transfer resistance values of the composite electrodes. Recently, Peng *et al.* synthesized an ultrathin CONs for fluorescence detection of DNA. They first prepared ultrathin TPA-COF nanosheets with a thickness of 3.5 ± 0.3 nm by solvent-assisted exfoliation. Then, two kinds of hairpin DNA probes (H1 and H2) were designed, and a fluorescent dye was utilized to mark H1. The fluorescence of the dye could be quenched when H1 and H2 were adsorbed on the TPA-COF NSs' surface as the result of the π-π stacking interactions between the surface and probe. A hybridization chain reaction (HCR) between H1 and H2 was triggered by the presence of target DNA,[180] producing a long double-stranded DNA (dsDNA) that showed poor interaction with COF nanosheets. Thus, the fluorescence of the dye could be recovered when the HCR-generated long dsDNA broke away from the TPA-COF nanosheets' surface, which enable the detection of target DNA.

4.4 Other applications

Besides the abovementioned applications, COF thin films can also be used in other fields such as catalyst[181-183] and drug delivery.[5] For example, Yadav *et al.* developed a triazine-based COF thin film on PI sheet as an efficient photocatalyst for solar fuel production from CO_2.[81] The newly designed COF thin films showed almost 3.7 times higher photocatalytic NADH regeneration and 3.4 times higher formic acid formation compared with that of the monomer. Polymeric structure, optical band gap and highly ordered π-electron channels enable the excellent performance of COF thin film photocatalyst. As another example, Yaghi and co-workers prepared a series of COF thin films with different electronic withdrawing characters by growing COF-366-Co, COF-366-$(OMe)_2$-Co, COF-366-F-Co and COF-366-$(F)_4$-Co on HOPG surface for electrocatalytic CO_2 reduction (Fig. 14).[182] The accessible and electrochemically active metal centers endow COF thin films with remarkably improved catalytic property over bulk COF powders. The XAS and cyclic voltammetry revealed that the electron withdrawing groups indeed enhanced the catalytic performance of the compounds though the current density for CO formation did not meet the linear trend of the electron withdrawing groups in materials.

Another graceful application of COF thin film is targeted drug delivery which has been presented by Banerjee *et al.*[5] While biocompatible polymers, nanomaterials and MOFs have been greatly used in the field of drug delivery, the shortages, such as poor chemical stability, released toxic metal ions, and limited functional design weaken their performance.[184, 185] COF thin films with metal-free, good aqueous dispersibility and designable function are qualified for drug delivery. Surface amine (-NH_2) groups are often used to anchor targeting ligands for site-specific drug delivery in targeted drug delivery system construction.[104, 186, 187] The authors elaborately chose TpASH with available hydroxyl (-OH) groups which are convenient to the bonding of surface amine (−NH_2) groups as well as the COF exfoliation.[72, 83] 5-Fluorouracil (5-FU) as an antimetabolite based anticancer chemotherapy drug was selected to be loaded onto the COF thin film surface.[188] The TpASH COF thin films loaded with the targeted drug 5-FU enabled the release of specific drug to cancer and was expected to minimize the unwanted side effects of nonspecific targeting. 5-FU loaded samples showed good anticancer activity, and only 14% of the

cells were viable at a dosage of 50 μg mL^{-1}. Targeted drug-loaded COF thin film (TpASH-FA-5-FU) preferentially delivered the drug (5-FU) to the folate over expressed breast cancer cells through receptor-mediated endocytosis that led to the cell death via apoptosis.

As a result, designable building backbones, adjustable thickness and accessible active sites enable COF thin films to have many enhanced features and functions, such as topological tunability, chemical stability, semiconducting behavior and improved capacitance, which would be beneficial for applications in energy storage, semiconductor devices, membrane separation, sensors and drug delivery. Moreover, other intriguing and/or unpredictable performance will be discovered and explored in the near future.

5. Outlook

From the above discussions, it is obvious that COF thin films inherit the merits of their bulk counterparts while possess some excellent new features. Bulk COF is usually synthesized as an insoluble powder which hinders its performance due to the poor processability.[38, 48, 125] Whereas COF thin films with single or few layers enable the strong interactions between molecules since their active sites are highly accessible on the surface and the synergistic effects of thin films and substrates also have advantages for improving their performance in various applications. Although some intriguing improvements have been made, this field is still in its infancy and several important challenges remain. As a prerequisite for device fabrication, it is of significant importance to seek for novel synthesis strategies, investigate the fundamental mechanism, and therefore expand their applications.

5.1 Synthetic strategy exploration

Although several strategies for fabricating COF thin film on selected substrates or as free-standing forms have been developed, simple but efficient synthesis strategies are always highly desirable. Among the currently existing methods related to bottom-up strategy, solvothermal synthesis is the most widely used method because of its easy operation feature. The problems in this method arise from two aspects. On the one hand, it is complicated to control the COF thin films thickness, and on the other hand the thin films are usually contaminated by precipitated COF powders, oligomers or unreacted monomers. While synthesis under flow conditions can avoid these problems by controlling the flow rate and tubing length, the lack of collecting and reusing monomers from outflow lead to serious waste of monomers. As for free-standing thin films, possible restacking impedes the obtainment of single or few layered COF thin films, let alone large lateral dimensions. And the crystallinity of them is also not high enough. As for both strategies, the yield of as-prepared COF thin films is too low for the practical applications. Hence, new synthesis methods equipped with scalability and morphology controllability need to be introduced. One of the feasible strategies is to combine two different methods. Such idea is very liberating that solvent-assisted exfoliation and mechanical delamination can be employed together to accelerate the reaction rate and increase the yield. Furthermore, methods used in other materials may also be suitable for COF thin film fabrication. For example, layer-by-layer templating technique have been widely used to synthesize nanostructured materials with different morphology for decades.[189-191] Recently, surface grafted gels (SURGELs), a kind of antimicrobial polymer thin films, were prepared by the deposition of surface anchored MOFs (SURMOFs) on gold substrates using the layer-by-layer method.[192] Considering that COFs have much in common with MOFs, layer-by-layer strategy are potential for COF thin film construction. Moreover, click reaction,[193] three-layer method[148] and facile surfactant-assisted synthesis method[194] are successfully used in MOF thin films fabrication. Likewise, these methods represent new opportunities to the fabrication of COF thin films with modified approach. For example, surfactant-assisted synthesis used in MOF thin films fabrication has its shortage that surfactants might occupy the active sites on thin films leading to a weak performance. In the future synthesis, surfactants that have weak interaction with COF thin films and can be washed after the reaction are preferred.

5.2 Mechanism study

While COF thin film has been widely studied not only in synthesis but also for applications, the fundamental mechanisms, such as growth orientation, crystallinity and occurrence of defects, are still far from clear. Indeed, very little is known about the conditions under which nucleation can be well controlled. And the growth orientation is critical that island growth may impede the obtainment of uniform and flat thin films. Meanwhile, the balance of thermodynamic of covalent bond formation, defect correction and interactions between COFs and substrates during the growth of COF thin films still remain to be decoded which are successfully achieved in well-developed polymers from irreversible reactions.[195, 196] In order to overcome these challenges, computational methods are very useful tools which enable the prediction of structure and function, as well as the simulation of stacking interactions and orientation growth. Dispersion-corrected density functional theory (DFT) was employed by Wang and co-workers[197] to investigate the interactions between a planar COF and graphene and clarify the assembly mechanism. The calculation results showed that COF network grows on graphene surface with an ordered hexagonal and square structure. On the other hand, computational methods make it possible to forecast the theoretical properties such as ion exchange, band gap and charge-carrier mobility which in reverse reflect the structural features.

Another strategy to speed up the progress of mechanism studies is the utilization of suitable characterization methods. In most studies, TEM and SEM images are used to analyse the morphology of COF thin films, whereas TEM is more likely to be employed to materials with heavier elements and SEM usually lacks the ability to assume the delicate surface morphology. As for PXRD, it gives only limited information about the crystal texture of COF thin films where precise conformations and positions of building blocks within the framework are absence.

On the other hand, GID and grazing incidence wide-angle X-ray scattering (GIWAXS) can provide detailed information of the orientation of thin films including out-of-plane and on-plane diffraction. These efficient techniques reveal more concrete information about the structure and orientation of thin film compared to that of TEM, SEM and PXRD. Very recently, Liu and co-workers[198] creatively used reaction time and concentration as effective handles to elucidate the intermediate state (the disoriented phase as well as disordered phase) during the process of COF thin films growth. An unusual re-entrant transition in orientation was observed using GIWAS for the first time. Advanced characteristic techniques are urgently needed to better understand the growth mechanism of COF thin films. Interestingly, new characteristic methods are conducive to learn more information about COF thin films growth, in reverse, the existing form of COF thin films enables the utilization of characterization that cannot be used in bulk COFs. For example, triphenylene-pyrene based TP-COF deposited on SLG/SiO_2 substrate made it possible to observe the COF thin films via UV/Vis/NIR spectroscopy in transmission mode.[53] And the optical property of LZU-1 COF thin films can be measured for the first time by ellipsometry.[75] What is worth mentioning is that the techniques used for other materials might also work for the study of COF thin films. For example, optical nano-imaging technique has been used to test the out-of-plane and in-plane dielectric constants of MoS_2 and h-BN crystals which shows a potential method to monitor the nanoscale optical quality of COF thin films.[199]

5.3 Application expansion

As mentioned above, COF thin films are highly desirable for the use of COFs in various applications. On the one hand, while COF thin films display enormous potential in electronic field, actual practice, such as portable electronics and hybrid electric vehicles, is far from mature, let alone large industrial equipment. Great efforts are still needed. On the other hand, up to now, a majority of COF thin films applications are limited to optoelectronic device, chemical sensors and membrane separation. The potential applications related to other fields are urgent to be developed, especially in the field of energy and environment. As known, energy shortage and environmental pollution restrict the development of modern society.[200-207] While lots of nanomaterials have been used,[208-215] it is sensible to utilize the pre-designable feature of COF thin films to bind various functional building blocks to broaden the applications. For example, N-rich frameworks are beneficial to CO_2 adsorption, and incorporating triazine-contained molecules allows COF thin films to have high CO_2 adsorption performance.[216, 217] Furthermore, COF thin films can act as 2D templates by introducing adsorbed molecules into the system which provides a strategy to form sophisticated functional surface, attracting considerable scientific attention in recent years.[218-220] COF thin films with high surface area and defined pore size are promising materials for templates. Interestingly, in the design of bulk COFs, heteropore COFs owning two or more types of pores are successfully achieved which can also be utilized in COF thin films fabrication.[221-224] Materials with the dual role of pollution detection and degradation are highly desirable in pollution abatement.[225-227] COF thin films with two different pore size favor this functional construction. Incorporating COF thin films into other materials is another potent strategy to produce multifunctional composites that have new properties overmatching those of individual moieties due to the synergetic effect and therefore enhance the application performance. Recently, Qiu and co-workers[228] grew a MOF on the COF membrane to synthesize a COF-MOF composite membrane. The as-prepared composite membrane possesses higher separation selectivity of H_2/CO_2 gas mixtures than individual parts. Under this consideration, constructing COF thin films with graphitic carbon nitride (g-C_3N_4) may enhance the ability of photocatalytic degradation of organic pollutants similar to h-BN/g-C_3N_4 composites.[229-234] Moreover, biological application is one of the important aspects for material application, which needs to pay close attention in the future. Pioneering studies have uncovered the great potential of COFs in biological field.[43, 44] Generally, COFs with total organic metal-free backbone rule out the unwanted toxic metals, and tunable porosity enables the convenience of loading guest/drug molecular.[5] But the poor dispersibility and unprocessable quality affect the biocompatibility and stability of bulk COF and further weak their performance. COF thin films with the high accessible surface, pronounced water stability and diversity function inspire us to hope for their better performance in biological field. Specifically, highly oriented COF thin films are beneficial for the loading with bioactive compounds which provide a platform for cell-culture substrates.[235-238] This also enables the biotransformation of surface-attached bacterial biofilms with small chemical compounds as well as spatially localized delivery of high concentrations of bioactive molecules such as antibiotics.

6. Conclusions

In summary, this critical review highlighted the accomplished synthesis of COF thin films deposited on selected substrates or as free-standing forms by using bottom-up and top-down strategies such as solvothermal synthesis, room temperature vapor-assisted conversion synthesis, solvent-assisted exfoliation, and mechanical delamination. Moreover, representative selections of COF thin film applications, like semiconductor devices and fluorescence sensors, were presented. In addition, future prospects with respect to synthetic strategy, mechanism and applications were provided. Despite the significant progress in this appealing research area, improved synthetic methods, well-dispersed nanosheets as well as diversified applications are urgently in need. Since this field is growing fast, what we can provide here is a momentary view. Nevertheless, we expect that this preliminary discussion will garner multidisciplinary interest from scientific research to industrial manufacture and therefore expand the future applications.

Abbreviation

[60]PCBM	[6,6]-Phenyl C61 butyric acid methyl ester
[70]PCBM	[6,6]-phenyl C71 butyric acid methyl ester
2D	Two-dimensional
3D	Three-dimensional
AFM	Atomic force microscopy
APH	4-aminobenzohydrazide
APTs	Active pharmaceutical ingredients
APTES	(3-Aminopropyl)triethoxysilane
ASH	4-aminosalicylhydrazide
BD	Benzidine
BDBA	1,4-benzenediboronic acid
BDH	Pyromellitic-N,N/-bisaminoimide
BDT	Benzodithiophene
BDTA	2,6-dicarbaldehyde-4,8-dioctyloxybenzo[1,2-b:3,4-b']dithiophene
BDTBA	Benzodithiophene diboronic acid
Boc	Tert-butyloxycarbonyl
Bpy	2,2'-bipyridine-5,5'-diamine
BTA	Benzene-1,3,5-tricarbaldehyde
BTPB	1,3,5-tris[4-phenylboroniacid]benzene
BSA	bovine serum albumin
CH_2Cl_2	Dichloromethane
CM	Curcumin
CMP	Conjugated microporous polymers
COFs	Covalent organic frameworks
COMs	COF membranes
CONs	COF nanosheets
dsDNA	Double-stranded deoxyribonucleic acid
Da	2,6-diaminoanthracene
DAAQ	Anthraquinone/ 2,6-diaminoanthraquinone
DAB	p-phenylenediamine
DCM	Dichloromethane
DFT	Density functional theory
DMF	N,N-Dimethylformamide
DNT	2,6-dinitrotoluene
DNP	2,6-dinitrophenol
DPB	4,4'-diphenylbutadiyl-ebis(boronic acid)
EB	Ethidium bromide
ECOFs	Exfoliated COFs
EIS	Electron impedance spectroscopy
EtOH	Alcohol
FA	Folic acid
FETs	Field-effect transistors
FT-IR	Fourier transform infrared spectroscopy
FTO	Fluorine doped tin oxide
FU	Fluorouracil
g-C3N4	Graphite carbon nitride
GCDC	Galvanostatic chargedischarge cycles
GID	Grazing incidence diffraction
GIWAXS	Grazing incidence wide-angle X-ray scattering
Glc	Glycidol
h-BN	Hexagonal boron nitride
HCR	Hybridization chain reaction
HHTP	2,3,6,7,10,11-hexahydroxytriphenylene
HODs	Hole-only devices
HRTEM	High-resolution TEM
IR	Infrared radiation
ITO	Indium-doped tin oxide
LED	Light-emitting diode
Li+	Lithium-ion
LiTFSI	Lithium bis(trifluoromethane) sulfonimide
LPE	Liquid Phase Exfoliation
MD	Molecular dynamics
MeOH	Methanol
MMMs	Mixed matrix membranes
MOFs	Metal-organic frameworks
MoS2	Molybdenum disulfide
NBDPA	4-(tert-butoxycarbonylamino)-aniline
NDI	Napthalenediimide
NF	Nanofltration
NiPc	Ni phthalocyanine
NP	2-nitrophenol
OLEDs	Organic Light-Emitting Diodes
OST	Octadecyltrichlorosilane
Pa	Benzene-1,4-diamine
PBBA	1,4-phenylene-bis(boronic acid)
PBI	Polybenzimidazole
PDA	p-phenylenediamine
PDBA	Pyrene-2,7-diboronic acid
PEMFCs	Proton-exchange membrane fuel cells
PES	Poly(ether sulfone)
PL	Photoluminescent
polyTp	conjugated 2D crystalline network based on tapa and bdta subunits
PPDA	p-phenylenediamine
PPE	Phenylbis(phenylethynyl)
PI	Polyimide
PSF	Polysulfone
PTCA	Perylenetracarboxylic dianhydride
PTSA	*p*-toluenesulfonic acid
PXRD	Powder x-ray diffraction
Py	Pyrene
QCM	Quartz crystal microbalance
RB	Rose Bengal
R-WT	Rhodamine WT
SAED	Selected area electron diffraction
SEM	Scanning electron microscopy
SLG	Single-layer graphene
SURGELs	Surface grafted gels
SURMOF	Surface anchored MOFs
TAPA	Tris(4-aminophenyl)amine
TAPB	1, 3, 5-tris(4-aminophenyl)benzene
TAPP	Tetra(4-aminophenyl)porphyrin
TCNQ	Tetracyanoquinodimethane
TD	4,4'-diamino-p-terphenyl
TEM	Transmission electron microscopy
TEMPO	(2,2,6,6-tetramethylpiperidin-1-yl)oxidanyl
TFC	Thin film composite
Tfp	1,3,5-tris(4-formylphenyl)benzene
TFP/Tp	1,3,5-triformylphluroglucinol
TFPA	Tris(4-formylphenyl)amine

TFPy	1,3,6,8-tetrakis(pformylphenyl)pyrene
TGx (X = Cl, Br, I)	A series of amines
THF	Tetrahydrofuran
TNP	2,4,6-trinitrophenol
TNT	2,4,6-trinitrotoluene
TP	Triphenylene-pyrene
TPA-COF	An imine-linked COF based on TAPA and TFPA
TPTC	Triptycene tricatechol
TPU	Thermoplastic polyurethanes
TTF	Tetrathiafulvalene
Ultem	Poly(ether imide)
UV/Vis/NIR	Ultraviolet/visible/near infrared
VFET	Vertical field-effect transistor
XPS	X-ray photoelectron spectroscopy
XRD	X-ray diffraction
ZnPc	Zn phthalocyanine

Conflicts of interest

There are no conflicts of interest to declare.

Acknowledgements

The study is financially supported by the Program for the National Natural Science Foundation of China (81773333, 51521006, 51709101, 51779090, 51579098, 51408206, 51508177, 51579096), the National Program for Support of Top–Notch Young Professionals of China (2014, 2012), Hunan Provincial Science and Technology Plan Project (No.2016RS3026, 2017SK2241), the Program for Changjiang Scholars and Innovative Research Team in University (IRT-13R17).

Notes and references

1. M.-H. Sun, S.-Z. Huang, L.-H. Chen, Y. Li, X.-Y. Yang, Z.-Y. Yuan and B.-L. Su, *Chemical Society reviews*, 2016, **45**, 3479-3563.
2. M. R. Benzigar, S. N. Talapaneni, S. Joseph, K. Ramadass, G. Singh, J. Scaranto, U. Ravon, K. Al-Bahily and A. Vinu, *Chemical Society reviews*, 2018, **47**, 2680-2721.
3. A. G. Slater and A. I. Cooper, *Science*, 2015, **348**, aaa8075.
4. S. Kitagawa, *Accounts Chem Res*, 2017, **50**, 514-516.
5. S. Mitra, H. S. Sasmal, T. Kundu, S. Kandambeth, K. Math, D. D. Diaz and R. Banerjee, *J Am Chem Soc*, 2017, **139**, 4513-4520.
6. L. X. Tan and B. Tan, *Chemical Society reviews*, 2017, **46**, 3322-3356.
7. Y. L. Luo, B. Y. Li, W. Wang, K. B. Wu and B. Tan, *Advanced materials*, 2012, **24**, 5703-5707.
8. Y. H. Xu, S. B. Jin, H. Xu, A. Nagai and D. L. Jiang, *Chemical Society reviews*, 2013, **42**, 8012-8031.
9. N. Chaoui, M. Trunk, R. Dawson, J. Schmidt and A. Thomas, *Chemical Society reviews*, 2017, **46**, 3302-3321.
10. Y. Z. Liao, Z. H. Cheng, W. W. Zuo, A. Thomas and C. F. J. Faul, *ACS applied materials & interfaces*, 2017, **9**, 38390-38400.
11. Y. Yuan, F. X. Sun, L. N. Li, P. Cui and G. S. Zhu, *Nature communications*, 2014, **5**.
12. K. Konstas, J. W. Taylor, A. W. Thornton, C. M. Doherty, W. X. Lim, T. J. Bastow, D. F. Kennedy, C. D. Wood, B. J. Cox, J. M. Hill, A. J. Hill and M. R. Hill, *Angew Chem Int Edit*, 2012, **51**, 6639-6642.
13. Y. Q. Li, T. Ben, B. Y. Zhang, Y. Fu and S. L. Qiu, *Scientific reports*, 2013, **3**.
14. A. Thomas, *Angew Chem Int Edit*, 2010, **49**, 8328-8344.
15. Y. G. Zhang and S. N. Riduan, *Chemical Society reviews*, 2012, **41**, 2083-2094.
16. P. Kaur, J. T. Hupp and S. T. Nguyen, *Acs Catal*, 2011, **1**, 819-835.
17. R. Dawson, A. I. Cooper and D. J. Adams, *Progress in Polymer Science*, 2012, **37**, 530-563.
18. T. Q. Ma, E. A. Kapustin, S. X. Yin, L. Liang, Z. Y. Zhou, J. Niu, L. H. Li, Y. Y. Wang, J. Su, J. Li, X. G. Wang, W. D. Wang, W. Wang, J. L. Sun and O. M. Yaghi, *Science*, 2018, **361**, 48-52.
19. B. M. Weckhuysen and J. H. Yu, *Chemical Society reviews*, 2015, **44**, 7022-7024.
20. Y. Li, H. X. Cao and J. H. Yu, *ACS nano*, 2018, **12**, 4096-4104.
21. H. Furukawa, K. E. Cordova, M. O'Keeffe and O. M. Yaghi, *Science*, 2013, **341**, 974-+.
22. M. Zhao, Y. Huang, Y. Peng, Z. Huang, Q. Ma and H. Zhang, *Chemical Society reviews*, 2018.
23. M. T. Zhao, K. Yuan, Y. Wang, G. D. Li, J. Guo, L. Gu, W. P. Hu, H. J. Zhao and Z. Y. Tang, *Nature*, 2016, **539**, 76-80.
24. G. Zhang, M. Tsujimoto, D. Packwood, N. T. Duong, Y. Nishiyama, K. Kadota, S. Kitagawa and S. Horike, *J Am Chem Soc*, 2018, **140**, 2602-2609.
25. Z. F. Pang, T. Y. Zhou, R. R. Liang, Q. Y. Qi and X. Zhao, *Chemical science*, 2017, **8**, 3866-3870.
26. C. S. Diercks and O. M. Yaghi, *Science*, 2017, **355**.
27. J. Zhang, X. Han, X. W. Wu, Y. Liu and Y. Cui, *J Am Chem Soc*, 2017, **139**, 8277-8285.
28. Q. R. Fang, Z. B. Zhuang, S. Gu, R. B. Kaspar, J. Zheng, J. H. Wang, S. L. Qiu and Y. S. Yan, *Nature communications*, 2014, **5**.
29. H. Xu, S. S. Tao and D. L. Jiang, *Nature materials*, 2016, **15**, 722-+.
30. A. P. Cote, A. I. Benin, N. W. Ockwig, M. O'Keeffe, A. J. Matzger and O. M. Yaghi, *Science*, 2005, **310**, 1166-1170.
31. F. J. Uribe-Romo, J. R. Hunt, H. Furukawa, C. Klock, M. O'Keeffe and O. M. Yaghi, *J Am Chem Soc*, 2009, **131**, 4570-+.
32. V. S. Vyas, M. Vishwakarma, I. Moudrakovski, F. Haase, G. Savasci, C. Ochsenfeld, J. P. Spatz and B. V. Lotsch, *Advanced materials*, 2016, **28**, 8749-8754.
33. S. Y. Ding, J. Gao, Q. Wang, Y. Zhang, W. G. Song, C. Y. Su and W. Wang, *J Am Chem Soc*, 2011, **133**, 19816-19822.
34. E. Vitaku and W. R. Dichtel, *J Am Chem Soc*, 2017, **139**, 12911-12914.
35. L. Stegbauer, K. Schwinghammer and B. V. Lotsch, *Chemical science*, 2014, **5**, 2789-2793.
36. F. J. Uribe-Romo, C. J. Doonan, H. Furukawa, K. Oisaki and O. M. Yaghi, *J Am Chem Soc*, 2011, **133**, 11478-11481.
37. S. Kandambeth, A. Mallick, B. Lukose, M. V. Mane, T. Heine and R. Banerjee, *J Am Chem Soc*, 2012, **134**, 19524-19527.
38. C. R. DeBlase, K. E. Silberstein, T. T. Truong, H. D. Abruna and W. R. Dichtel, *J Am Chem Soc*, 2013, **135**, 16821-16824.
39. W. T. Liu, Q. Su, P. Y. Ju, B. X. Guo, H. Zhou, G. H. Li and Q. L. Wu, *ChemSusChem*, 2017, **10**, 664-669.

40. J. H. Sun, A. Klechikov, C. Moise, M. Prodana, M. Enachescu and A. V. Talyzin, *Angew Chem Int Edit*, 2018, **57**, 1034-1038.
41. Z. A. Ghazi, L. Y. Zhu, H. Wang, A. Naeem, A. M. Khattak, B. Liang, N. A. Khan, Z. X. Wei, L. S. Li and Z. Y. Tang, *Adv Energy Mater*, 2016, **6**.
42. A. M. Khattak, Z. A. Ghazi, B. Liang, N. A. Khan, A. Iqbal, L. S. Li and Z. Y. Tang, *Journal of Materials Chemistry A*, 2016, **4**, 16312-16317.
43. L. Y. Bai, S. Z. F. Phua, W. Q. Lim, A. Jana, Z. Luo, H. P. Tham, L. Z. Zhao, Q. Gao and Y. L. Zhao, *Chem Commun*, 2016, **52**, 4128-4131.
44. Q. R. Fang, J. H. Wang, S. Gu, R. B. Kaspar, Z. B. Zhuang, J. Zheng, H. X. Guo, S. L. Qiu and Y. S. Yan, *J Am Chem Soc*, 2015, **137**, 8352-8355.
45. L. Meri-Bofi, S. Royuela, F. Zamora, M. L. Ruiz-Gonzalez, J. L. Segura, R. Munoz-Olivas and M. J. Mancheno, *Journal of Materials Chemistry A*, 2017, **5**, 17973-17981.
46. Y. F. Zeng, R. Y. Zou, Z. Luo, H. C. Zhang, X. Yao, X. Ma, R. Q. Zou and Y. L. Zhao, *J Am Chem Soc*, 2015, **137**, 1020-1023.
47. H. L. Qian, C. X. Yang and X. P. Yan, *Nature communications*, 2016, **7**.
48. S. Lin, C. S. Diercks, Y. B. Zhang, N. Kornienko, E. M. Nichols, Y. B. Zhao, A. R. Paris, D. Kim, P. Yang, O. M. Yaghi and C. J. Chang, *Science*, 2015, **349**, 1208-1213.
49. S. Bhunia, S. K. Das, R. Jana, S. C. Peter, S. Bhattacharya, M. Addicoat, A. Bhaumik and A. Pradhan, *ACS applied materials & interfaces*, 2017, **9**, 23843-23851.
50. N. Keller, D. Bessinger, S. Reuter, M. Calik, L. Ascherl, F. C. Hanusch, F. Auras and T. Bein, *J Am Chem Soc*, 2017, **139**, 8194-8199.
51. S. Dalapati, S. B. Jin, J. Gao, Y. H. Xu, A. Nagai and D. L. Jiang, *J Am Chem Soc*, 2013, **135**, 17310-17313.
52. S. Kitagawa and R. Matsuda, *Coordination Chemistry Reviews*, 2007, **251**, 2490-2509.
53. J. W. Colson, A. R. Woll, A. Mukherjee, M. P. Levendorf, E. L. Spitler, V. B. Shields, M. G. Spencer, J. Park and W. R. Dichtel, *Science*, 2011, **332**, 228-231.
54. S. Park and R. S. Ruoff, *Nature nanotechnology*, 2009, **4**, 217-224.
55. Y. Zhang, G. M. Zeng, L. Tang, J. Chen, Y. Zhu, X. X. He and Y. He, *Anal Chem*, 2015, **87**, 989-996.
56. K. S. Novoselov, A. K. Geim, S. V. Morozov, D. Jiang, Y. Zhang, S. V. Dubonos, I. V. Grigorieva and A. A. Firsov, *Science*, 2004, **306**, 666-669.
57. C. Lai, M. M. Wang, G. M. Zeng, Y. G. Liu, D. L. Huang, C. Zhang, R. Z. Wang, P. Xu, M. Cheng, C. Huang, H. P. Wu and L. Qin, *Appl Surf Sci*, 2016, **390**, 368-376.
58. D. L. Huang, X. Wang, C. Zhang, G. M. Zeng, Z. W. Peng, J. Zhou, M. Cheng, R. Z. Wang, Z. X. Hu and X. Qin, *Chemosphere*, 2017, **186**, 414-421.
59. I. Berlanga, M. L. Ruiz-Gonzalez, J. M. Gonzalez-Calbet, J. L. G. Fierro, R. Mas-Balleste and F. Zamora, *Small*, 2011, **7**, 1207-1211.
60. R. P. Bisbey and W. R. Dichtel, *ACS central science*, 2017, **3**, 533-543.
61. A. I. Cooper, *Crystengcomm*, 2013, **15**, 1483-1483.
62. N. Huang, P. Wang and D. L. Jiang, *Nature Reviews Materials*, 2016, **1**.
63. C. R. DeBlase and W. R. Dichtel, *Macromolecules*, 2016, **49**, 5297-5305.
64. S. Y. Ding and W. Wang, *Chemical Society reviews*, 2013, **42**, 548-568.
65. C. Y. Lin, D. T. Zhang, Z. H. Zhao and Z. H. Xia, *Advanced materials*, 2018, **30**.
66. X. H. Liu, C. Z. Guan, D. Wang and L. J. Wan, *Advanced materials*, 2014, **26**, 6912-6920.
67. X. S. Li, Y. W. Zhu, W. W. Cai, M. Borysiak, B. Y. Han, D. Chen, R. D. Piner, L. Colombo and R. S. Ruoff, *Nano letters*, 2009, **9**, 4359-4363.
68. E. L. Spitler, B. T. Koo, J. L. Novotney, J. W. Colson, F. J. Uribe-Romo, G. D. Gutierrez, P. Clancy and W. R. Dichtel, *J Am Chem Soc*, 2011, **133**, 19416-19421.
69. E. L. Spitler, J. W. Colson, F. J. Uribe-Romo, A. R. Woll, M. R. Giovino, A. Saldivar and W. R. Dichtel, *Angew Chem Int Edit*, 2012, **51**, 2623-2627.
70. D. D. Medina, V. Werner, F. Auras, R. Tautz, M. Dogru, J. Schuster, S. Linke, M. Doblinger, J. Feldmann, P. Knochel and T. Bein, *ACS nano*, 2014, **8**, 4042-4052.
71. S. L. Cai, Y. B. Zhang, A. B. Pun, B. He, J. H. Yang, F. M. Toma, I. D. Sharp, O. M. Yaghi, J. Fan, S. R. Zheng, W. G. Zhang and Y. Liu, *Chemical Science*, 2014, **5**, 4693-4700.
72. C. R. DeBlase, K. Hernandez-Burgos, K. E. Silberstein, G. G. Rodriguez-Calero, R. P. Bisbey, H. D. Abruna and W. R. Dichtel, *ACS nano*, 2015, **9**, 3178-3183.
73. X. H. Gou, Q. Zhang, Y. L. Wu, Y. J. Zhao, X. F. Shi, X. Fan, L. Z. Huang and G. Li, *Rsc Adv*, 2016, **6**, 39198-39203.
74. S. Kandambeth, A. Mallick, B. Lukose, M. V. Mane, T. Heine and R. Banerjee, *J Am Chem Soc*, 2012, **134**, 19524-19527.
75. Y. B. Zhao, L. Guo, F. Gandara, Y. H. Ma, Z. Liu, C. H. Zhu, H. Lu, C. A. Trickett, E. A. Kapustin, O. Terasaki and O. M. Yaghi, *J Am Chem Soc*, 2017, **139**, 13166-13172.
76. S. Karan, Z. W. Jiang and A. G. Livingston, *Science*, 2015, **348**, 1347-1351.
77. M. F. Jimenez-Solomon, Q. L. Song, K. E. Jelfs, M. Munoz-Ibanez and A. G. Livingston, *Nature materials*, 2016, **15**, 760-+.
78. R. Matsuoka, R. Sakamoto, K. Hoshiko, S. Sasaki, H. Masunaga, K. Nagashio and H. Nishihara, *J Am Chem Soc*, 2017, **139**, 3145-3152.
79. J. I. Feldblyum, C. H. McCreery, S. C. Andrews, T. Kurosawa, E. J. G. Santos, V. Duong, L. Fang, A. L. Ayzner and Z. N. Bao, *Chem Commun*, 2015, **51**, 13894-13897.
80. W. Y. Dai, F. Shao, J. Szczerbinski, R. McCaffrey, R. Zenobi, Y. H. Jin, A. D. Schluter and W. Zhang, *Angew Chem Int Edit*, 2016, **55**, 213-217.
81. K. Dey, M. Pal, K. C. Rout, H. S. Kunjattu, A. Das, R. Mukherjee, U. K. Kharul and R. Banerjee, *J Am Chem Soc*, 2017, **139**, 13083-13091.
82. M. Matsumoto, L. Valentino, G. M. Stiehl, H. B. Balch, A. R. Corcos, F. Wang, D. C. Ralph, B. J. Marinas and W. R. Dichtel, *Chem-Us*, 2018, **4**, 308-317.
83. D. D. Medina, J. M. Rotter, Y. H. Hu, M. Dogru, V. Werner, F. Auras, J. T. Markiewicz, P. Knochel and T. Bein, *J Am Chem Soc*, 2015, **137**, 1016-1019.
84. R. P. Bisbey, C. R. DeBlase, B. J. Smith and W. R. Dichtel, *J Am Chem Soc*, 2016, **138**, 11433-11436.
85. I. Berlanga, R. Mas-Balleste and F. Zamora, *Chem Commun*, 2012, **48**, 7976-7978.
86. D. N. Bunck and W. R. Dichtel, *J Am Chem Soc*, 2013, **135**, 14952-14955.

87. Y. W. Peng, Y. Huang, Y. H. Zhu, B. Chen, L. Y. Wang, Z. C. Lai, Z. C. Zhang, M. T. Zhao, C. L. Tan, N. L. Yang, F. W. Shao, Y. Han and H. Zhang, *J Am Chem Soc*, 2017, **139**, 8698-8704.
88. G. Li, K. Zhang and T. Tsuru, *ACS applied materials & interfaces*, 2017, **9**, 8433-8436.
89. Y. Hernandez, V. Nicolosi, M. Lotya, F. M. Blighe, Z. Y. Sun, S. De, I. T. McGovern, B. Holland, M. Byrne, Y. K. Gun'ko, J. J. Boland, P. Niraj, G. Duesberg, S. Krishnamurthy, R. Goodhue, J. Hutchison, V. Scardaci, A. C. Ferrari and J. N. Coleman, *Nature nanotechnology*, 2008, **3**, 563-568.
90. A. P. Cote, H. M. El-Kaderi, H. Furukawa, J. R. Hunt and O. M. Yaghi, *J Am Chem Soc*, 2007, **129**, 12914-+.
91. S. D. Bergin, V. Nicolosi, P. V. Streich, S. Giordani, Z. Y. Sun, A. H. Windle, P. Ryan, N. P. P. Niraj, Z. T. T. Wang, L. Carpenter, W. J. Blau, J. J. Boland, J. P. Hamilton and J. N. Coleman, *Advanced materials*, 2008, **20**, 1876-+.
92. H. Zhang, *ACS nano*, 2015, **9**, 9451-9469.
93. J. X. Jiang, F. Su, A. Trewin, C. D. Wood, H. Niu, J. T. A. Jones, Y. Z. Khimyak and A. I. Cooper, *J Am Chem Soc*, 2008, **130**, 7710-7720.
94. S. Chandra, S. Kandambeth, B. P. Biswal, B. Lukose, S. M. Kunjir, M. Chaudhary, R. Babarao, T. Heine and R. Banerjee, *J Am Chem Soc*, 2013, **135**, 17853-17861.
95. B. P. Biswal, S. Chandra, S. Kandambeth, B. Lukose, T. Heine and R. Banerjeet, *J Am Chem Soc*, 2013, **135**, 5328-5331.
96. S. Wang, Q. Y. Wang, P. P. Shao, Y. Z. Han, X. Gao, L. Ma, S. Yuan, X. J. Ma, J. W. Zhou, X. Feng and B. Wang, *J Am Chem Soc*, 2017, **139**, 4258-4261.
97. X. W. Mu, J. Zhan, X. M. Feng, B. H. Yuan, S. L. Qiu, L. Song and Y. Hu, *ACS applied materials & interfaces*, 2017, **9**, 23017-23026.
98. A. L. Qu, X. M. Xu, Y. Y. Zhang, Y. Y. Li, W. Y. Zha, S. W. Wei, H. L. Xie and J. X. Wang, *React Funct Polym*, 2016, **102**, 93-100.
99. N. Huang, X. S. Ding, J. Kim, H. Ihee and D. L. Jiang, *Angew Chem Int Edit*, 2015, **54**, 8704-8707.
100. L. Ascherl, T. Sick, J. T. Margraf, S. H. Lapidus, M. Calik, C. Hettstedt, K. Karaghiosoff, M. Doblinger, T. Clark, K. W. Chapman, F. Auras and T. Bein, *Nature chemistry*, 2016, **8**, 310-316.
101. M. A. Khayum, S. Kandambeth, S. Mitra, S. B. Nair, A. Das, S. S. Nagane, R. Mukherjee and R. Banerjee, *Angew Chem Int Edit*, 2016, **55**, 15604-15608.
102. E. R. Thapaliya, B. Captain and F. M. Raymo, *Journal of Organic Chemistry*, 2014, **79**, 3973-3981.
103. L. Ji, G. N. Guo, H. Y. Sheng, S. L. Qin, B. W. Wang, D. D. Han, T. T. Li, D. Yang and A. G. Dong, *Chemistry of Materials*, 2016, **28**, 3823-3830.
104. T. R. Cook, Y. R. Zheng and P. J. Stang, *Chemical reviews*, 2013, **113**, 734-777.
105. Z. Kahveci, T. Islamoglu, G. A. Shar, R. Ding and H. M. El-Kaderi, *Crystengcomm*, 2013, **15**, 1524-1527.
106. T. Y. Zhou, F. Lin, Z. T. Li and X. Zhao, *Macromolecules*, 2013, **46**, 7745-7752.
107. S. Mitra, S. Kandambeth, B. P. Biswal, M. A. Khayum, C. K. Choudhury, M. Mehta, G. Kaur, S. Banerjee, A. Prabhune, S. Verma, S. Roy, U. K. Kharu and R. Banerjee, *J Am Chem Soc*, 2016, **138**, 2823-2828.
108. K. Baek, G. Yun, Y. Kim, D. Kim, R. Hota, I. Hwang, D. Xu, Y. H. Ko, G. H. Gu, J. H. Suh, C. G. Park, B. J. Sung and K. Kim, *J Am Chem Soc*, 2013, **135**, 6523-6528.
109. B. J. Smith, L. R. Parent, A. C. Overholts, P. A. Beaucage, R. P. Bisbey, A. D. Chavez, N. Hwang, C. Park, A. M. Evans, N. C. Gianneschi and W. R. Dichtel, *ACS central science*, 2017, **3**, 58-65.
110. G. Das, T. Skorjanc, S. K. Sharma, F. Gandara, M. Lusi, D. S. S. Rao, S. Vimala, S. K. Prasad, J. Raya, D. S. Han, R. Jagannathan, J. C. Olsen and A. Trabolsi, *J Am Chem Soc*, 2017, **139**, 9558-9565.
111. C. Zhong, Y. D. Deng, W. B. Hu, J. L. Qiao, L. Zhang and J. J. Zhang, *Chemical Society reviews*, 2015, **44**, 7484-7539.
112. V. Etacheri, R. Marom, R. Elazari, G. Salitra and D. Aurbach, *Energy & Environmental Science*, 2011, **4**, 3243-3262.
113. S. Ummartyotin and Y. Infahsaeng, *Renew Sust Energ Rev*, 2016, **55**, 17-24.
114. Y. Z. Liao, H. G. Wang, M. F. Zhu and A. Thomas, *Advanced materials*, 2018, **30**.
115. L. F. Gao, S. Y. Gan, H. Y. Li, D. X. Han, F. H. Li, Y. Bao and L. Niu, *Nanotechnology*, 2017, **28**.
116. M. R. Gerhardt, L. C. Tong, R. Gomez-Bombarelli, Q. Chen, M. P. Marshak, C. J. Galvin, A. Aspuru-Guzik, R. G. Gordon and M. J. Aziz, *Adv Energy Mater*, 2017, **7**.
117. G. Pognon, T. Brousse and D. Belanger, *Carbon*, 2011, **49**, 1340-1348.
118. X. Chen, H. W. Wang, H. Yi, X. F. Wang, X. R. Yan and Z. H. Guo, *J Phys Chem C*, 2014, **118**, 8262-8270.
119. G. Pognon, T. Brousse, L. Demarconnay and D. Belanger, *J Power Sources*, 2011, **196**, 4117-4122.
120. M. Le Comte, T. Brousse and D. Belanger, *Electrochim Acta*, 2014, **137**, 447-453.
121. J. Q. Zha, L. R. Xu, Z. K. Wang, X. G. Li, Q. M. Pan, P. G. Hu and S. B. Lei, *ACS applied materials & interfaces*, 2015, **7**, 27837-17843.
122. C. Montoro, D. Rodriguez-San-Miguel, E. Polo, R. Escudero-Cid, M. L. Ruiz-Gonzalez, J. A. R. Navarro, P. Ocon and F. Zamora, *J Am Chem Soc*, 2017, **139**, 10079-10086.
123. J. Wang, L. Si, Q. Wei, X. Hong, S. Cai and Y. Cai, *ACS Applied Nano Materials*, 2017, **1**, 132-138.
124. A. K. Mandal, J. Mahmood and J. B. Baek, *Chemnanomat*, 2017, **3**, 373-391.
125. J. G. Mei, Y. Diao, A. L. Appleton, L. Fang and Z. N. Bao, *J Am Chem Soc*, 2013, **135**, 6724-6746.
126. J. L. Segura and N. Martin, *Angew Chem Int Edit*, 2001, **40**, 1372-1409.
127. H. M. Ding, Y. H. Li, H. Hu, Y. M. Sun, J. G. Wang, C. X. Wang, C. Wang, G. X. Zhang, B. S. Wang, W. Xu and D. Q. Zhang, *Chem-Eur J*, 2014, **20**, 14614-14618.
128. G. H. V. Bertrand, V. K. Michaelis, T. C. Ong, R. G. Griffin and M. Dinca, *Proceedings of the National Academy of Sciences of the United States of America*, 2013, **110**, 4923-4928.
129. C. Poelking, M. Tietze, C. Elschner, S. Olthof, D. Hertel, B. Baumeier, F. Wurthner, K. Meerholz, K. Leo and D. Andrienko, *Nature materials*, 2015, **14**, 434-439.
130. A. Mishra and P. Bauerle, *Angew Chem Int Edit*, 2012, **51**, 2020-2067.
131. Y. S. Liu, C. C. Chen, Z. R. Hong, J. Gao, Y. Yang, H. P. Zhou, L. T. Dou, G. Li and Y. Yang, *Scientific reports*, 2013, **3**.
132. D. D. Medina, M. L. Petrus, A. N. Jumabekov, J. T. Margraf, S. Weinberger, J. M. Rotter, T. Clark and T. Bein, *ACS nano*, 2017, **11**, 2706-2713.
133. D. Braga and G. Horowitz, *Advanced materials*, 2009, **21**, 1473-1486.

134. F. Dinelli, M. Murgia, P. Levy, M. Cavallini, F. Biscarini and D. M. de Leeuw, *Physical review letters*, 2004, **92**.
135. B. Sun, C. H. Zhu, Y. Liu, C. Wang, L. J. Wan and D. Wang, *Chemistry of Materials*, 2017, **29**, 4367-4374.
136. A. J. Ben-Sasson and N. Tessler, *Nano letters*, 2012, **12**, 4729-4733.
137. R. S. Haszeldine, *Science*, 2009, **325**, 1647-1652.
138. D. J. Miller, D. R. Dreyer, C. W. Bielawski, D. R. Paul and B. D. Freeman, *Angew Chem Int Edit*, 2017, **56**, 4662-4711.
139. J. G. Duan, W. Q. Jin and S. Kitagawa, *Coordination Chemistry Reviews*, 2017, **332**, 48-74.
140. L. Ding, Y. Y. Wei, L. B. Li, T. Zhang, H. H. Wang, J. Xue, L. X. Ding, S. Q. Wang, J. Caro and Y. Gogotsi, *Nature communications*, 2018, **9**.
141. X. R. Wang, C. L. Chi, K. Zhang, Y. H. Qian, K. M. Gupta, Z. X. Kang, J. W. Jiang and D. Zhao, *Nature communications*, 2017, **8**.
142. J. S. Zhang, J. A. Schott, Y. C. Li, W. C. Zhan, S. M. Mahurin, K. Nelson, X. G. Sun, M. P. Paranthaman and S. Dai, *Advanced materials*, 2017, **29**.
143. J. R. Werber, C. O. Osuji and M. Elimelech, *Nature Reviews Materials*, 2016, **1**.
144. S. P. Koenig, L. D. Wang, J. Pellegrino and J. S. Bunch, *Nature nanotechnology*, 2012, **7**, 728-732.
145. J. T. Chen, C. C. Shih, Y. J. Fu, S. H. Huang, C. C. Hu, K. R. Lee and J. Y. Lai, *Industrial & Engineering Chemistry Research*, 2014, **53**, 2781-2789.
146. X. L. Cui, K. J. Chen, H. B. Xing, Q. W. Yang, R. Krishna, Z. B. Bao, H. Wu, W. Zhou, X. L. Dong, Y. Han, B. Li, Q. L. Ren, M. J. Zaworotko and B. L. Chen, *Science*, 2016, **353**, 141-144.
147. A. Cadiau, K. Adil, P. M. Bhatt, Y. Belmabkhout and M. Eddaoudi, *Science*, 2016, **353**, 137-140.
148. T. Rodenas, I. Luz, G. Prieto, B. Seoane, H. Miro, A. Corma, F. Kapteijn, F. X. L. I. Xamena and J. Gascon, *Nature materials*, 2015, **14**, 48-55.
149. J. F. Yao and H. T. Wang, *Chemical Society reviews*, 2014, **43**, 4470-4493.
150. Z. X. Kang, M. Xue, L. L. Fan, L. Huang, L. J. Guo, G. Y. Wei, B. L. Chen and S. L. Qiu, *Energy & Environmental Science*, 2014, **7**, 4053-4060.
151. Z. P. Lai, G. Bonilla, I. Diaz, J. G. Nery, K. Sujaoti, M. A. Amat, E. Kokkoli, O. Terasaki, R. W. Thompson, M. Tsapatsis and D. G. Vlachos, *Science*, 2003, **300**, 456-460.
152. Y. Y. Zhang, X. Feng, H. W. Li, Y. F. Chen, J. S. Zhao, S. Wang, L. Wang and B. Wang, *Angew Chem Int Edit*, 2015, **54**, 4259-4263.
153. S. Kandambeth, B. P. Biswal, H. D. Chaudhari, K. C. Rout, H. S. Kunjattu, S. Mitra, S. Karak, A. Das, R. Mukherjee, U. K. Kharul and R. Banerjee, *Advanced materials*, 2017, **29**.
154. K. Zhang, Z. J. He, K. M. Gupta and J. W. Jiang, *Environ Sci-Wat Res*, 2017, **3**, 735-743.
155. L. Valentino, M. Matsumoto, W. R. Dichtel and B. J. Marinas, *Environmental Science & Technology*, 2017, **51**, 14352-14359.
156. H. W. Fan, J. H. Gu, H. Meng, A. Knebel and J. Caro, *Angew Chem Int Edit*, 2018, **57**, 4083-4087.
157. M. M. Tong, Q. Y. Yang, Q. T. Ma, D. H. Liu and C. L. Zhong, *Journal of Materials Chemistry A*, 2016, **4**, 124-131.
158. Y. Peng, Y. S. Li, Y. J. Ban, H. Jin, W. M. Jiao, X. L. Liu and W. S. Yang, *Science*, 2014, **346**, 1356-1359.
159. H. Li, Z. N. Song, X. J. Zhang, Y. Huang, S. G. Li, Y. T. Mao, H. J. Ploehn, Y. Bao and M. Yu, *Science*, 2013, **342**, 95-98.
160. H. W. Kim, H. W. Yoon, S. M. Yoon, B. M. Yoo, B. K. Ahn, Y. H. Cho, H. J. Shin, H. Yang, U. Paik, S. Kwon, J. Y. Choi and H. B. Park, *Science*, 2013, **342**, 91-95.
161. J. R. Li, J. Sculley and H. C. Zhou, *Chemical reviews*, 2012, **112**, 869-932.
162. Y. W. Peng, G. D. Xu, Z. G. Hu, Y. D. Cheng, C. L. Chi, D. Q. Yuan, H. S. Cheng and D. Zhao, *ACS applied materials & interfaces*, 2016, **8**, 18505-18512.
163. X. Y. Wu, Z. Z. Tian, S. F. Wang, D. D. Peng, L. X. Yang, Y. Z. Wu, Q. P. Xin, H. Wu and Z. Y. Jiang, *Journal of Membrane Science*, 2017, **528**, 273-283.
164. X. Cao, Z. Qiao, Z. Wang, S. Zhao, P. Li, J. Wang and S. Wang, *International Journal of Hydrogen Energy*, 2016, **41**, 9167-9174.
165. M. Shan, B. Seoane, E. Rozhko, A. Dikhtiarenko, G. Clet, F. Kapteijn and J. Gascon, *Chemistry*, 2016, **22**, 14467-14470.
166. Z. X. Kang, Y. W. Peng, Y. H. Qian, D. Q. Yuan, M. A. Addicoat, T. Heine, Z. G. Hu, L. Tee, Z. G. Guo and D. Zhao, *Chemistry of Materials*, 2016, **28**, 1277-1285.
167. L. M. Robeson, *Journal of Membrane Science*, 2008, **320**, 390-400.
168. D. Bessinger, L. Ascherl, F. Auras and T. Bein, *J Am Chem Soc*, 2017, **139**, 12035-12042.
169. M. R. Rao, Y. Fang, S. De Feyter and D. F. Perepichka, *J Am Chem Soc*, 2017, **139**, 2421-2427.
170. H. Wang, Y. Li, T. Chen, L. S. Li, T. Fang and Z. Y. Tang, *J Mater Chem C*, 2015, **3**, 5136-5140.
171. C. Q. Lin, H. M. Ding, D. Q. Yuan, B. S. Wang and C. Wang, *J Am Chem Soc*, 2016, **138**, 3302-3305.
172. Q. Sun, B. Aguila, J. Perman, L. D. Earl, C. W. Abney, Y. C. Cheng, H. Wei, N. Nguyen, L. Wojtas and S. Q. Ma, *J Am Chem Soc*, 2017, **139**, 2786-2793.
173. X. Li, Q. Gao, J. F. Wang, Y. F. Chen, Z. H. Chen, H. S. Xu, W. Tang, K. Leng, G. H. Ning, J. S. Wu, Q. H. Xu, S. Y. Quek, Y. X. Lu and K. P. Loh, *Nature communications*, 2018, **9**.
174. B. Joarder, A. V. Desai, P. Samanta, S. Mukherjee and S. K. Ghosh, *Chem-Eur J*, 2015, **21**, 965-969.
175. K. Wollin and H. H. Dieter, *Archives of environmental contamination and toxicology*, 2005, **49**, 18-26.
176. J. F. Wyman, M. P. Serve, D. W. Hobson, L. H. Lee and D. E. Uddin, *Journal of toxicology and environmental health*, 1992, **37**, 313-327.
177. G. Das, B. P. Biswal, S. Kandambeth, V. Venkatesh, G. Kaur, M. Addicoat, T. Heine, S. Verma and R. Banerjee, *Chemical science*, 2015, **6**, 3931-3939.
178. C. L. Zhang, S. M. Zhang, Y. H. Yan, F. Xia, A. N. Huang and Y. Z. Xian, *ACS applied materials & interfaces*, 2017, **9**, 13415-13421.
179. P. Y. Wang, M. M. Kang, S. M. Sun, Q. Liu, Z. H. Zhang and S. M. Fang, *Chinese J Chem*, 2014, **32**, 838-843.
180. R. M. Dirks and N. A. Pierce, *Proceedings of the National Academy of Sciences of the United States of America*, 2004, **101**, 15275-15278.
181. R. K. Yadav, A. Kumar, N. J. Park, K. J. Kong and J. O. Baeg, *Journal of Materials Chemistry A*, 2016, **4**, 9413-9418.
182. C. S. Diercks, S. Lin, N. Komienko, E. A. Kapustin, E. M. Nichols, C. H. Zhu, Y. B. Zhao, C. J. Chang and O. M. Yaghi, *J Am Chem Soc*, 2018, **140**, 1116-1122.
183. T. Sick, A. G. Hufnagel, J. Kampmann, I. Kondofersky, M. Calik, J. M. Rotter, A. Evans, M. Doblinger, S. Herbert, K. Peters, D. Bohm, P. Knochel, D. D. Medina, D. Fattakhova-Rohlfing and T. Bein, *J Am Chem Soc*, 2018, **140**, 2085-2092.

184. P. Horcajada, T. Chalati, C. Serre, B. Gillet, C. Sebrie, T. Baati, J. F. Eubank, D. Heurtaux, P. Clayette, C. Kreuz, J. S. Chang, Y. K. Hwang, V. Marsaud, P. N. Bories, L. Cynober, S. Gil, G. Ferey, P. Couvreur and R. Gref, *Nature materials*, 2010, **9**, 172-178.
185. H. Alhmoud, B. Delalat, R. Elnathan, A. Cifuentes-Rius, A. Chaix, M. L. Rogers, J. O. Durand and N. H. Voelcker, *Adv Funct Mater*, 2015, **25**, 1137-1145.
186. M. S. Lohse, T. Stassin, G. Naudin, S. Wuttke, R. Ameloot, D. De Vos, D. D. Medina and T. Bein, *Chemistry of Materials*, 2016, **28**, 626-631.
187. H. Xu, J. Gao and D. L. Jiang, *Nature chemistry*, 2015, **7**, 905-912.
188. C. C. Liang, A. Y. Park and J. L. Guan, *Nat Protoc*, 2007, **2**, 329-333.
189. Y. Wang, A. S. Angelatos and F. Caruso, *Chemistry of Materials*, 2008, **20**, 848-858.
190. O. Shekhah, H. Wang, S. Kowarik, F. Schreiber, M. Paulus, M. Tolan, C. Sternemann, F. Evers, D. Zacher, R. A. Fischer and C. Woll, *J Am Chem Soc*, 2007, **129**, 15118-+.
191. J. B. Hoffmann, G. Zaiats, I. Wappes and P. V. Kamat, *Chemistry of Materials*, 2017, **29**, 9767-9774.
192. W. C. Zhou, S. Begum, Z. B. Wang, P. Krolla, D. Wagner, S. Brase, C. Woll and M. Tsotsalas, *ACS applied materials & interfaces*, 2018, **10**, 1528-1533.
193. Y. Goto, H. Sato, S. Shinkai and K. Sada, *J Am Chem Soc*, 2008, **130**, 14354-+.
194. M. T. Zhao, Y. X. Wang, Q. L. Ma, Y. Huang, X. Zhang, J. F. Ping, Z. C. Zhang, Q. P. Lu, Y. F. Yu, H. Xu, Y. L. Zhao and H. Zhang, *Advanced materials*, 2015, **27**, 7372-+.
195. G. Carrot, S. Diamanti, M. Manuszak, B. Charleux and I. P. Vairon, *J Polym Sci Pol Chem*, 2001, **39**, 4294-4301.
196. G. Moad, E. Rizzardo and S. H. Thang, *Polymer*, 2008, **49**, 1079-1131.
197. R. N. Gunasinghe, D. G. Reuven, K. Suggs and X. Q. Wang, *Journal of Physical Chemistry Letters*, 2012, **3**, 3048-3052.
198. H. Wang, B. He, F. Liu, C. Stevens, M. A. Brady, S. Cai, C. Wang, T. P. Russell, T. W. Tan and Y. Liu, *J Mater Chem C*, 2017, **5**, 5090-5095.
199. D. B. Hu, X. X. Yang, C. Li, R. N. Liu, Z. H. Yan, H. Hu, S. N. G. Corder, J. N. Chen, Z. P. Sun, M. Y. Liu and Q. Dai, *Nature communications*, 2017, **8**.
200. D. H. Zhang, J. Q. Wang, Y. G. Lu, Y. L. Si, C. Huang, J. Yang, B. Huang and W. Li, *Renew Sust Energ Rev*, 2017, **76**, 865-871.
201. M. Chen, P. Xu, G. M. Zeng, C. P. Yang, D. L. Huang and J. C. Zhang, *Biotechnol Adv*, 2015, **33**, 745-755.
202. X. Y. Ren, G. M. Zeng, L. Tang, J. J. Wang, J. Wan, Y. N. Liu, J. F. Yu, H. Yi, S. J. Ye and R. Deng, *Sci Total Environ*, 2018, **610**, 1154-1163.
203. M. Cheng, G. M. Zeng, D. L. Huang, C. Lai, P. Xu, C. Zhang and Y. Liu, *Chem Eng J*, 2016, **284**, 582-598.
204. X. Y. Guo, Z. W. Peng, D. L. Huang, P. Xu, G. M. Zeng, S. Zhou, X. M. Gong, M. Cheng, R. Deng, H. Yi, H. Luo, X. L. Yan and T. Li, *Chem Eng J*, 2018, **347**, 74-83.
205. C. J. Hu, D. L. Huang, G. M. Zeng, M. Cheng, X. M. Gong, R. Z. Wang, W. J. Xue, Z. X. Hu and Y. N. Liu, *Chem Eng J*, 2018, **338**, 432-439.
206. D. L. Huang, L. S. Liu, G. M. Zeng, P. Xu, C. Huang, L. J. Deng, R. Z. Wang and J. Wan, *Chemosphere*, 2017, **174**, 545-553.
207. S. P. Bao, H. Wang, W. C. Zhang, Z. C. Xie and T. Fang, *Environ Pollut*, 2016, **219**, 696-704.
208. J. Wan, G. M. Zeng, D. L. Huang, L. Hu, P. Xu, C. Huang, R. Deng, W. J. Xue, C. Lai, C. Y. Zhou, K. X. Zheng, X. Y. Ren and X. M. Gong, *J Hazard Mater*, 2018, **343**, 332-339.
209. C. Zhang, C. Lai, G. M. Zeng, D. L. Huang, C. P. Yang, Y. Wang, Y. Y. Zhou and M. Cheng, *Water Res*, 2016, **95**, 103-112.
210. X. Gong, D. L. Huang, Y. G. Liu, Z. W. Peng, G. M. Zeng, P. Xu, M. Cheng, R. Z. Wang and J. Wan, *Crit Rev Biotechnol*, 2018, **38**, 455-468.
211. H. Yi, D. Huang, L. Qin, G. Zeng, C. Lai, M. Cheng, S. Ye, B. Song, X. Ren and X. Guo, *Applied Catalysis B: Environmental*, 2018, **239**, 408-424.
212. D. L. Huang, Z. X. Hu, Z. W. Peng, G. M. Zeng, G. M. Chen, C. Zhang, M. Cheng, J. Wan, X. Wang and X. Qin, *J Environ Manage*, 2018, **210**, 191-200.
213. D. L. Huang, W. J. Xue, G. M. Zeng, J. Wan, G. M. Chen, C. Huang, C. Zhang, M. Cheng and P. A. Xu, *Water Res*, 2016, **106**, 15-25.
214. D. L. Huang, X. Qin, Z. W. Peng, Y. G. Liu, X. M. Gong, G. M. Zeng, C. Huang, M. Cheng, W. J. Xue, X. Wang and Z. X. Hu, *Ecotox Environ Safe*, 2018, **153**, 229-237.
215. W. J. Xue, D. L. Huang, G. M. Zeng, J. Wan, C. Zhang, R. Xu, M. Cheng and R. Deng, *J Hazard Mater*, 2018, **341**, 381-389.
216. K. X. Yao, Y. L. Chen, Y. Lu, Y. F. Zhao and Y. Ding, *Carbon*, 2017, **122**, 258-265.
217. J. Du, Y. Liu, P. Krishna, Y. Yu, Y. Cui, S. Wang, Y. Liu, X. Song and Z. Liang, *ACS applied materials & interfaces*, 2018.
218. J. A. Berrocal, J. Teyssandier, O. J. G. M. Goor, S. De Feyter and E. W. Meijer, *Chemistry of Materials*, 2018, **30**, 3372-3378.
219. M. Zhan and Y. Tian, *Accounts Chem Res*, 2018, **51**, 688-696.
220. C. Hadad, X. X. Ke, M. Carraro, A. Sartorel, C. Bittencourt, G. Van Tendeloo, M. Bonchio, M. Quintana and M. Prato, *Chem Commun*, 2014, **50**, 885-887.
221. C. Qian, S. Q. Xu, G. F. Jiang, T. G. Zhan and X. Zhao, *Chem-Eur J*, 2016, **22**, 17784-17789.
222. T. Y. Zhou, S. Q. Xu, Q. Wen, Z. F. Pang and X. Zhao, *J Am Chem Soc*, 2014, **136**, 15885-15888.
223. C. Qian, Q. Y. Qi, G. F. Jiang, F. Z. Cui, Y. Tian and X. Zhao, *J Am Chem Soc*, 2017, **139**, 6736-6743.
224. Y. P. Mo, X. H. Liu and D. Wang, *ACS nano*, 2017, **11**, 11694-11700.
225. P. A. Xu, G. M. Zeng, D. L. Huang, C. L. Feng, S. Hu, M. H. Zhao, C. Lai, Z. Wei, C. Huang, G. X. Xie and Z. F. Liu, *Sci Total Environ*, 2012, **424**, 1-10.
226. W. W. Tang, G. M. Zeng, J. L. Gong, J. Liang, P. Xu, C. Zhang and B. B. Huang, *Sci Total Environ*, 2014, **468**, 1014-1027.
227. H. L. Qian, C. Dai, C. X. Yang and X. P. Yan, *ACS applied materials & interfaces*, 2017, **9**, 24999-25005.
228. J. R. Fu, S. Das, G. L. Xing, T. Ben, V. Valtchev and S. L. Qiu, *J Am Chem Soc*, 2016, **138**, 7673-7680.
229. W. J. Ong, L. L. Tan, Y. H. Ng, S. T. Yong and S. P. Chai, *Chemical reviews*, 2016, **116**, 7159-7329.
230. L. B. Jiang, X. Z. Yuan, G. M. Zeng, Z. B. Wu, J. Liang, X. H. Chen, L. J. Leng, H. Wang and H. Wang, *Appl Catal B-Environ*, 2018, **221**, 715-725.
231. C. Y. Zhou, C. Lai, D. L. Huang, G. M. Zeng, C. Zhang, M. Cheng, L. Hu, J. Wan, W. P. Xiong, M. Wen, X. F. Wen and L. Qin, *Appl Catal B-Environ*, 2018, **220**, 202-210.
232. W. Wang, P. Xu, M. Chen, G. Zeng, C. Zhang, C. Zhou, Y. Yang, D. Huang, C. Lai, M. Cheng, L. Hu, W. Xiong, H. Guo

and M. Zhou, *ACS Sustainable Chemistry & Engineering*, 2018, **6**, 15503-15516.
233. C. Zhou, C. Lai, P. Xu, G. Zeng, D. Huang, Z. Li, C. Zhang, M. Cheng, L. Hu, J. Wan, F. Chen, W. Xiong and R. Deng, *ACS Sustainable Chemistry & Engineering*, 2018, **6**, 6941-6949.
234. C. Y. Zhou, C. Lai, C. Zhang, G. M. Zeng, D. L. Huang, M. Cheng, L. Hu, W. P. Xiong, M. Chen, J. J. Wang, Y. Yang and L. B. Jiang, *Appl Catal B-Environ*, 2018, **238**, 6-18.
235. G. K. Such, A. P. R. Johnston and F. Caruso, *Chemical Society reviews*, 2011, **40**, 19-29.
236. S. Wuttke, D. D. Medina, J. M. Rotter, S. Begum, T. Stassin, R. Ameloot, M. Oschatz and M. Tsotsalas, *Adv Funct Mater*, 2018, **28**, 1801545.
237. H. Y. Zhao, Z. Jin, H. M. Su, X. F. Jing, F. X. Sun and G. S. Zhu, *Chem Commun*, 2011, **47**, 6389-6391.
238. M. Tsotsalas, J. Liu, B. Tettmann, S. Grosjean, A. Shahnas, Z. Wang, C. Azucena, M. Addicoat, T. Heine, J. Lahann, J. Overhage, S. Brase, H. Gliemann and C. Woll, *J Am Chem Soc*, 2014, **136**, 8-11.
239. Y. Chen, H. J. Cui, J. Q. Zhang, K. Zhao, D. F. Ding, J. Guo, L. S. Li, Z. Y. Tian and Z. Y. Tang, *Rsc Adv*, 2015, **5**, 92573-92576.
240. S. Wang, Q. Wang, P. Shao, Y. Han, X. Gao, L. Ma, S. Yuan, X. Ma, J. Zhou and X. Feng, *J Am Chem Soc*, 2017, **139**, 4258-4261.

Journal Name

ARTICLE

Table 1. COF thin films on different substrates with controllable thickness for various applications.

COF	Substrates (interface)	Fabrication method	Thickness (nm)	Applications	Ref.
COF-5	SLG/Cu	Solvothermal synthesis	193 ± 20[a]		53
	SLG/SiO_2		35 ± 5[b]		
	SLG/SiC		73 ± 4[c]		
NiPc-PBBA COF	SLG/SiO_2		210 ± 25	Semiconductor devices	
HHTP-DPB COF	SLG/SiO_2	Solvothermal synthesis	132 ± 18	Fluorescent sensors	68
ZnPc-Py COF	SLG/SiO_2	Solvothermal synthesis	400 ± 12		69
ZnPc-NDI COF			580 ± 84		
ZnPc-PPE COF			200 ± 18		
ZnPc-DPB COF			296 ± 6		
BDT-COF	ITO-coated glass	Solvothermal synthesis	150		70
	NiO/ITO-coated glass		150		
	Au				
	SiO_2		150		
TTF-COF	Si/SiO_2	Solvothermal synthesis	150		71
	ITO-coated glass		150		
$COF_{DAAQ-BTA}$	3D graphene	Solvothermal synthesis	180	Capacitive Electrode	121
DAAQ-TFP COF	Au	Solvothermal synthesis	200[d]	Supercapacitors	72
polyTB	Mother liquor solution/air	Interfacial synthesis	2-200	FETs	79
BDT-COF	Glass	Room temperature vapor-assisted conversion	300		83
DAB-TFP COF	ITO-coated glass	Solvothermal synthesis	200		73
COF-5	QCM	Synthesis under continuous flow conditions			84
$COF_{TFPy-PPDA}$	SLG	Solvothermal synthesis	50	FETs	135
LZU-1	Si	Solvothermal synthesis	190		75
BDT-COF	Glass-coated indium-doped ITO	Solvothermal synthesis	200	Semiconductor materials	132
COF-LZU1	Si–SiO2	Solvothermal synthesis			198

	Si–APTES		423		
	Si–OTS				
TT-COF	Glass-substrate	Solvothermal synthesis	200	Photoelectric device	239
TAPB-PDA COF	PES	Interfacial synthesis	10.4 ± 2.6[e]	NF membrane	82, 155
BDT-ETTA COF	FTO/ITO	Solvothermal synthesis	100-500	Photocathodes	183
COF-366-Co	HOPG	Solvothermal synthesis	250	Electrocatalyst	182
Py-tTII COF	ITO transparent electrodes	Solvothermal synthesis	450	NIR photodetector	168
Tp-Bpy COF	Dichloromethane/water	Interfacial synthesis	160 ± 10	NF membrane-separeation	81
Tp-Azo COF			150 ± 10		
Tp-Ttba COF			130 ± 10		
Tp-Tta COF			190 ± 10		
CTF	Polyimide	Solvothermal synthesis	35.1	Photocatalyst	181
Polyimine network	Air/water	Interfacial synthesis	0.7		80

[a, b, c] Different growth time; [d] The thickness can be varied by the change of initial monomer concentration; [e] 1 COF layer.

Table 2. Free-standing COF thin films with different thickness for various applications.

COF	Fabrication methods	Thickness (nm)	Applications	Ref.
COF-8	Solvent-assisted exfoliation	4-10		59
CMP-0	Solvent-assisted exfoliation	2.4 ± 0.2[a]		85
COF-43	Solvent-assisted exfoliation	1.32 ± 0.37		86
TpPa	Mechanical delamination	3-10		94
TpBD				
$COF_{BDBA-TPTC}$	Self-exfoliation method	0.75		106
$COF_{BPDBA-TPTC}$		0.72		
TpTGx[b]	Self-exfoliation method	2-5	iCONs@Polysulfone (PSF) MMMs	107
DaTp	Chemical exfoliation	5-6[c]		101
DAAQ-ECOF	Mechanical delamination	3-5	Cathode Materials for Lithium-Ion Batteries	240
TpASH	Chemical exfoliation	15	Drug delivery	5
COF (melamine-OPA)	Mechanical delamination		TPU/COFs Nanocomposites	97
TPA-COF	Solvent-assisted exfoliation	3.5 ± 0.3	DNA detection	87
TpBDH	Solvent-assisted exfoliation	1.5-5.1		177
TfpBDH			Chemical sensing	
COF-1	Solvent-assisted exfoliation	0.5	Molecular sieving membranes	88

[a] After 120 min sonication; [b] X = Cl^-, Br^-, I^-; [c] Medium DaTp-CONs concentration.

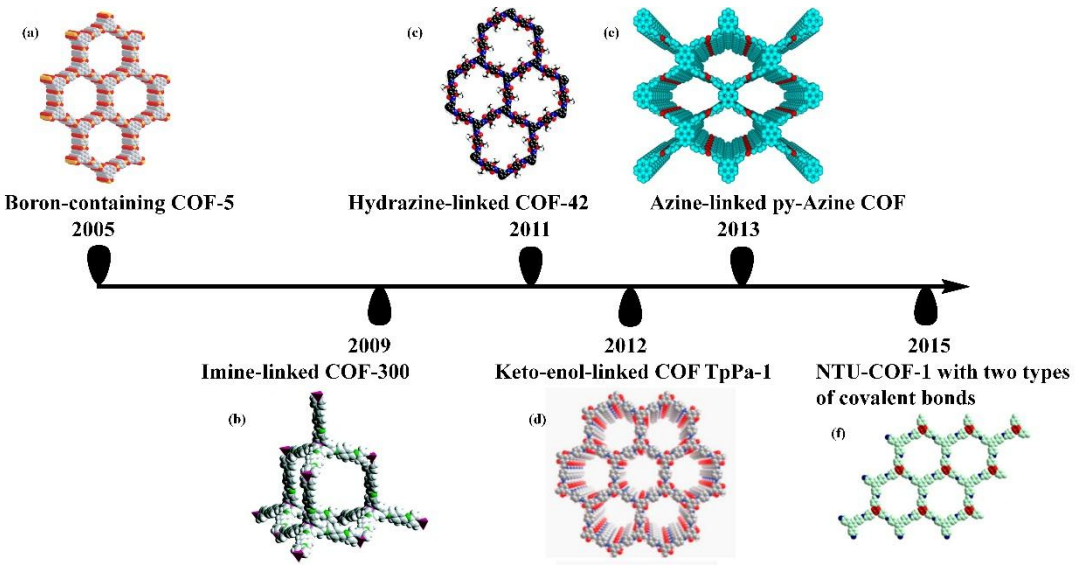

Fig. 1 Selected examples of existing COFs with different covalent linkages. (a) Boron-containing COF-5. Reproduced with permission from ref. 30. Copyright 2005, American Association for the Advancement of Science. (b) Imine-linked COF-300. Reproduced with permission from ref. 31. Copyright 2009, American Chemical Society. (c) Hydrazine-linked COF-42. Reproduced with permission from ref. 36. Copyright 2011, American Chemical Society. (d) Keto-enol-linked COF TpPa-1. Reproduced with permission from ref. 37. Copyright 2012, American Chemical Society. (e) Azine-linked Py-Azine COF. Reproduced with permission from ref. 51. Copyright 2013, American Chemical Society. (f) NTU-COF-1 with two types of covalent bonds. Reproduced with permission from ref. 46. Copyright 2015, American Chemical Society.

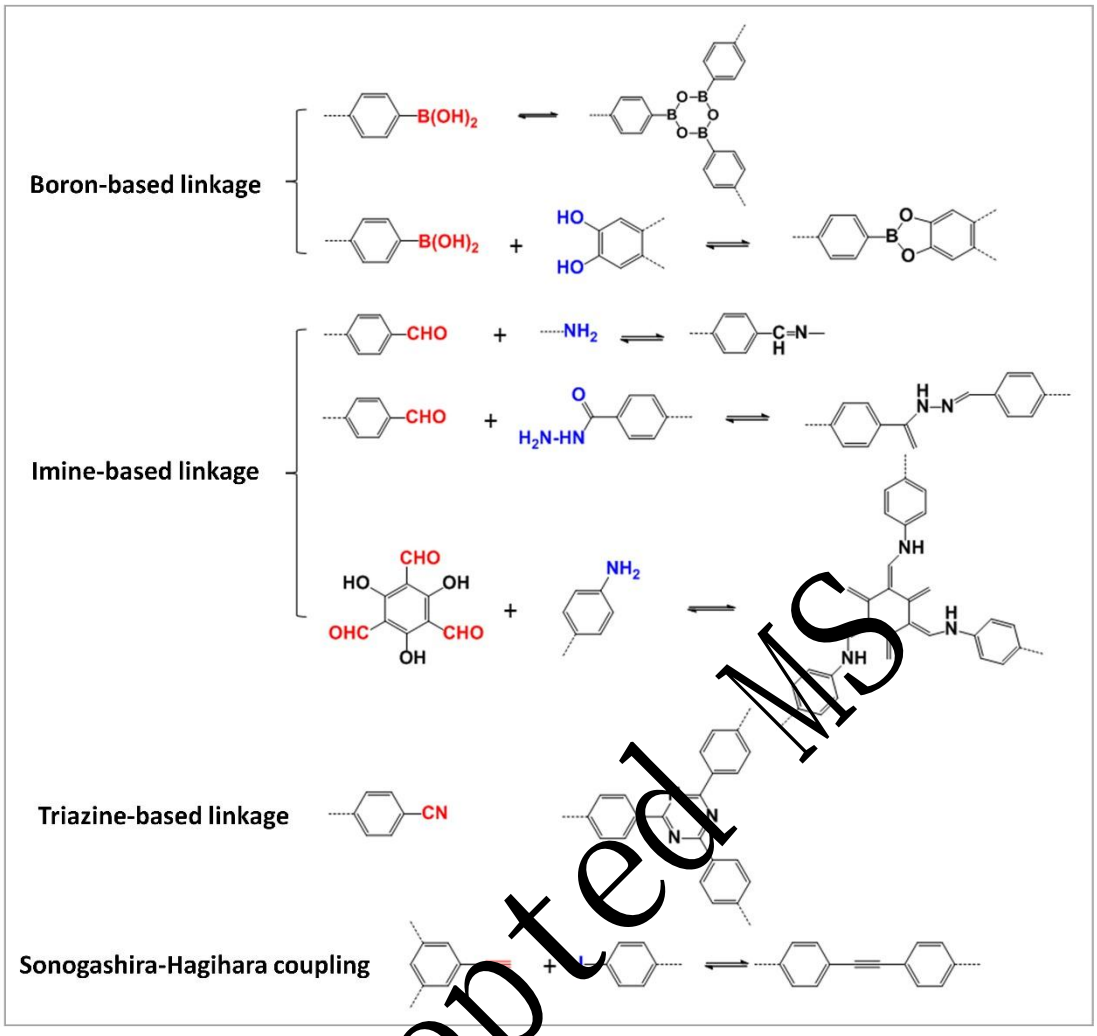

Fig. 2 Versatile linkages involved in the COF thin films formation comprising boron-based linkage (boroxine and boronate ester), imine-based linkage (for example, hydrazine and β-ketoenamine), triazine-based linkage and Sonogashira-Hagihara coupling.

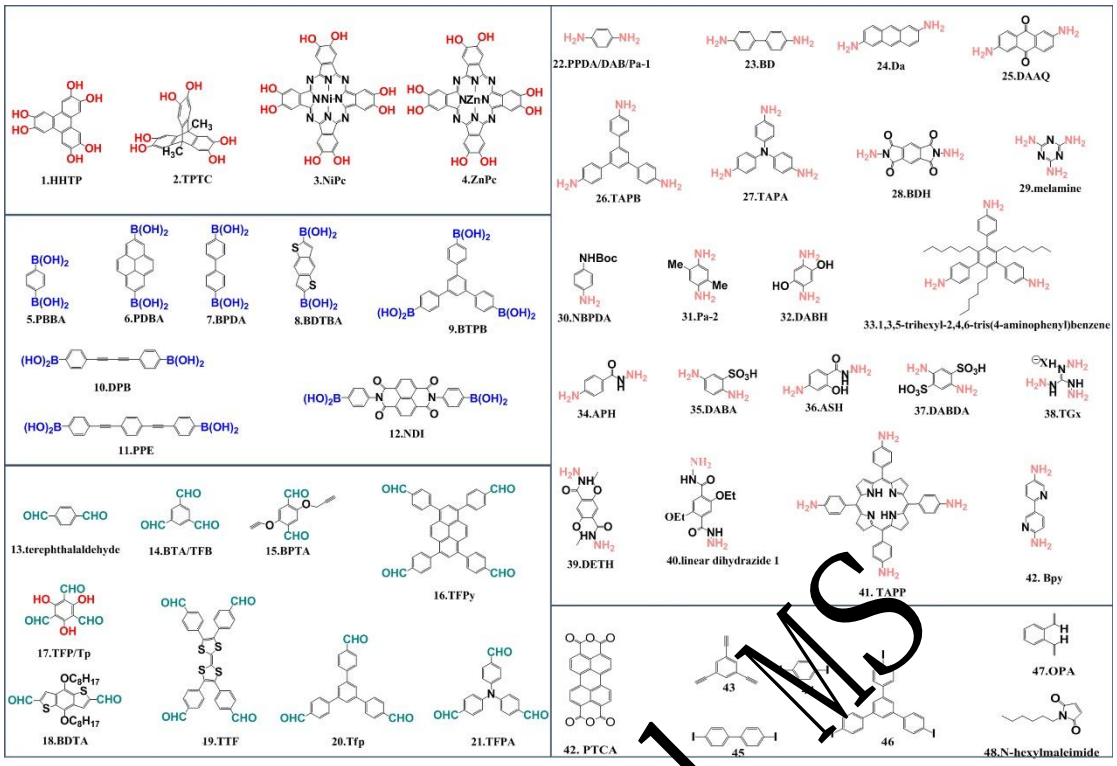

Fig. 3 Building blocks bearing catechol, boronic acid, aldehyde, amine and other units involved in the COF thin films formation.

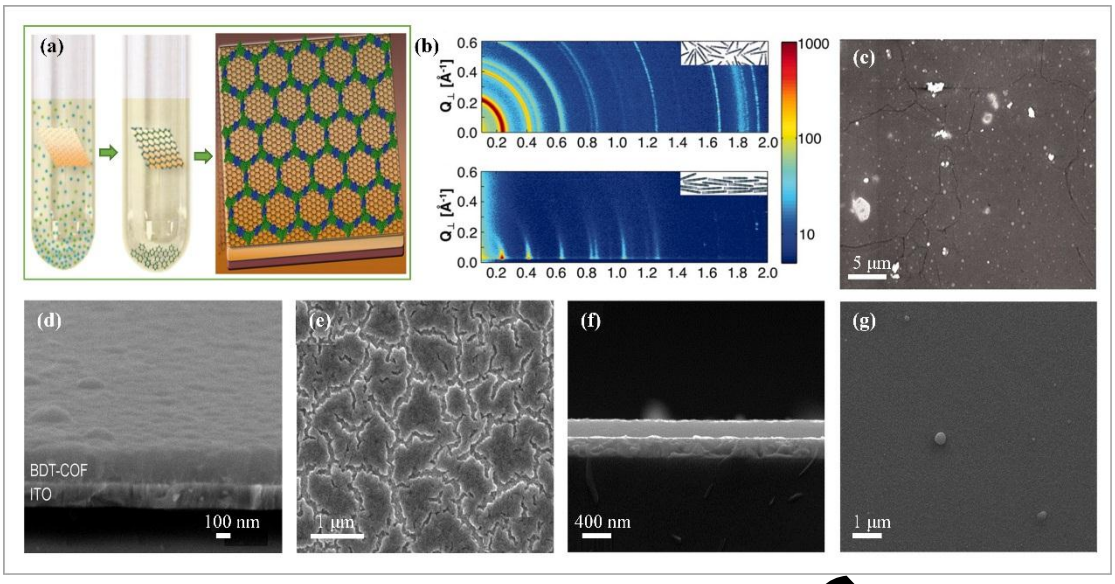

Fig. 4 (a) Schematic illustration of the solvothermal synthesis of COF-5 thin films. (b) X-ray scattering data of COF-5 powder (inset: schematic of randomly oriented COF-5 grains in the powder). (b) GID data from a COF-5 film on SLG/Cu (inset: schematic of oriented COF-5 grains in the film. (c) Top-view SEM image of the COF-5 thin film. Reproduced with permission from ref. 53. Copyright 2011, American Association for the Advancement of Science. (d) Cross-section SEM image of the BDT-COF thin film on ITO-coated glass. (e) Top-view SEM image of the BDT-COF thin film on ITO-coated glass. Reproduced with permission from ref. 78. Copyright 2014, American Chemical Society. (f) Top-view SEM image of the DAB-TFP COF thin film on ITO-coated glass. (g) Cross-section SEM image of the DAB-TFP COF thin film on ITO-coated glass. Reproduced with permission from ref. 73. Copyright 2016, Royal Society of Chemistry.

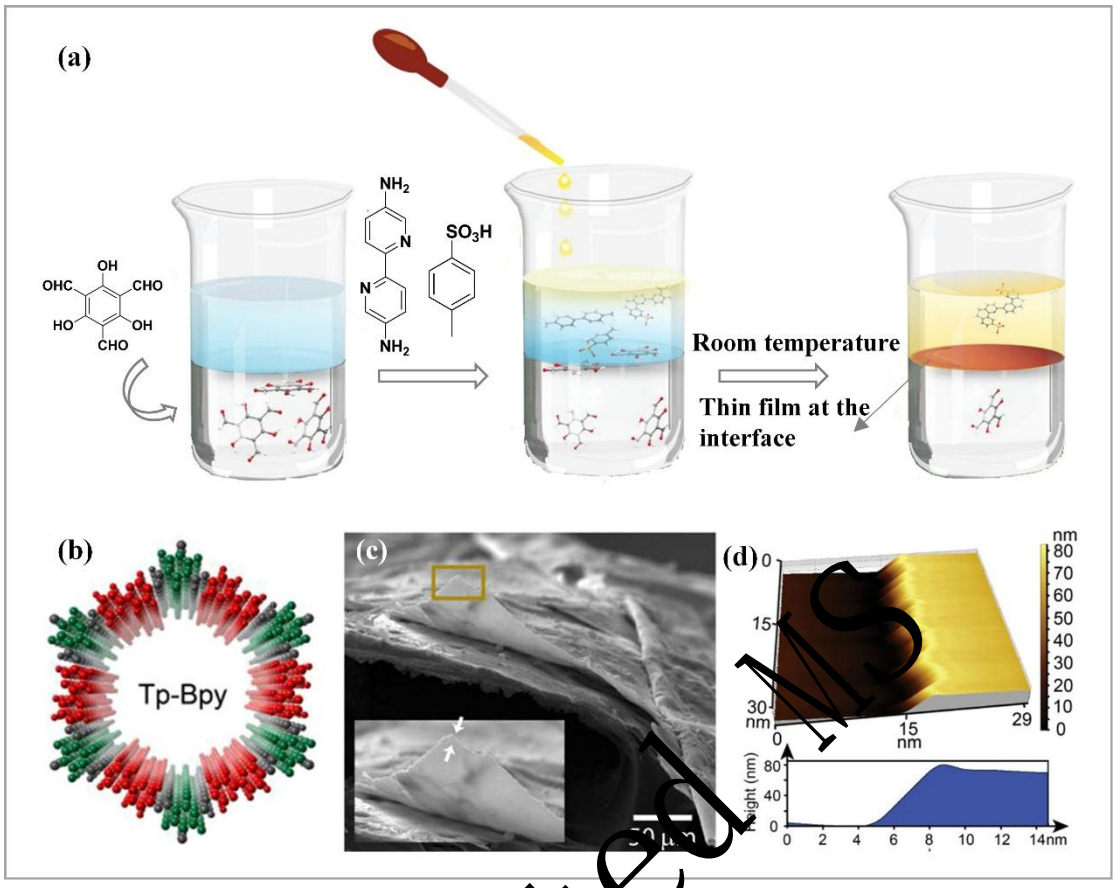

Fig. 5 (a) Schematic illustration of the interfacial synthesis of Tp-Bpy COF thin films. (b) AA stacking mode of Tp-Bpy COF. (c) SEM image of Tp-Bpy COF thin films. (d) AFM image of Tp-Bpy COF thin films. Reproduced with permission from ref. 81. Copyright 2014, American Chemical Society.

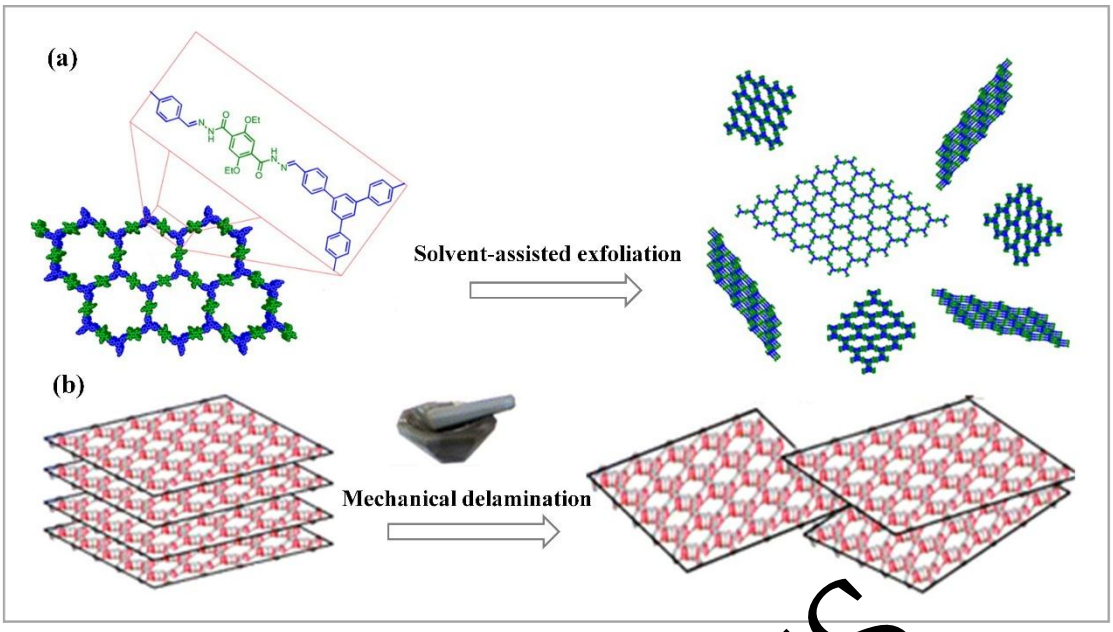

Fig. 6 (a) Scheme of the solvent-assisted exfoliation of COF-43. Reproduced with permission from ref. 86. Copyright 2013, American Chemical Society. (b) Schematic representation of the mechanical delamination of TpPa COF. Reproduced with permission from ref. 94. Copyright 2013, American Chemical Society.

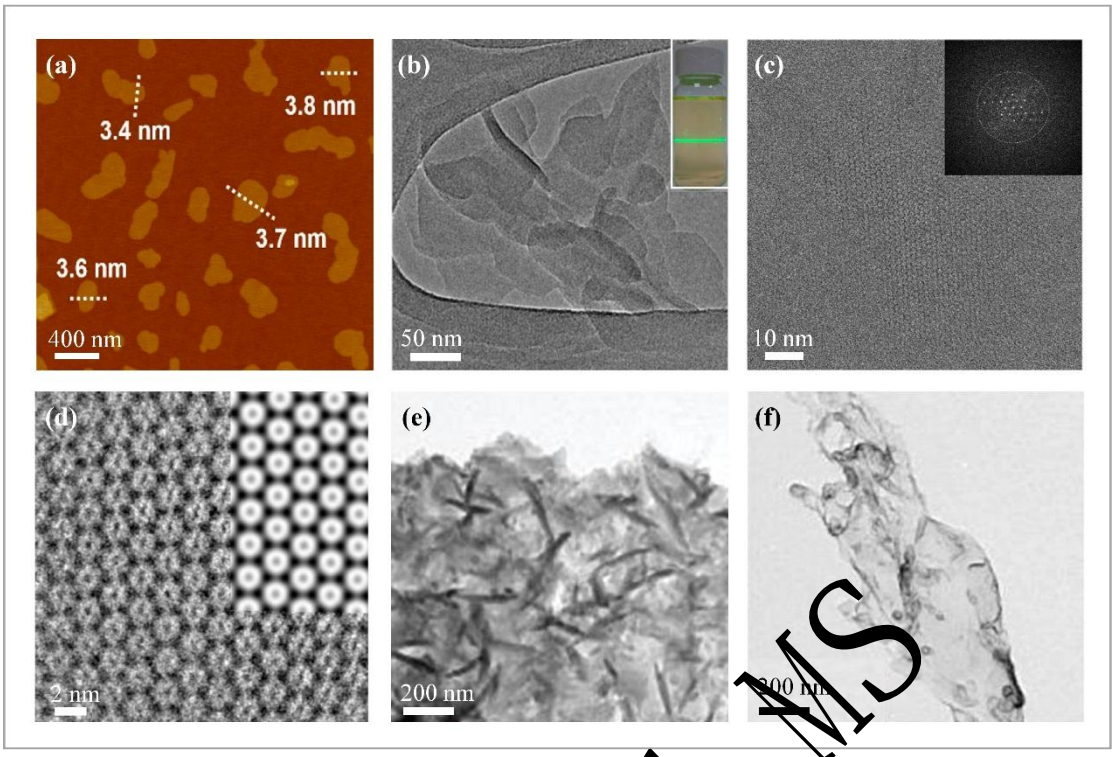

Fig. 7 (a) AFM image of TPA-COF nanosheets with the thickness indicated. (2) TEM image of TPA-COF nanosheets with an inset photograph of the Tyndall effect of the TPA-COF nanosheets suspension. (c) Low-dose high-resolution motion-corrected TEM image of the TPA-COF nanosheets with an inset of characterization of the fast Fourier transform (FFT). (d) Enlarged HRTEM image with an inset of simulated HRTEM image. Reproduced with permission from ref. 87. Copyright 2017, American Chemical Society. (e) HRTEM image of TpPa-2 before grinding. (f) HRTEM image of TpPa-2 after grinding. Reproduced with permission from ref. 94. Copyright 2013, American Chemical Society.

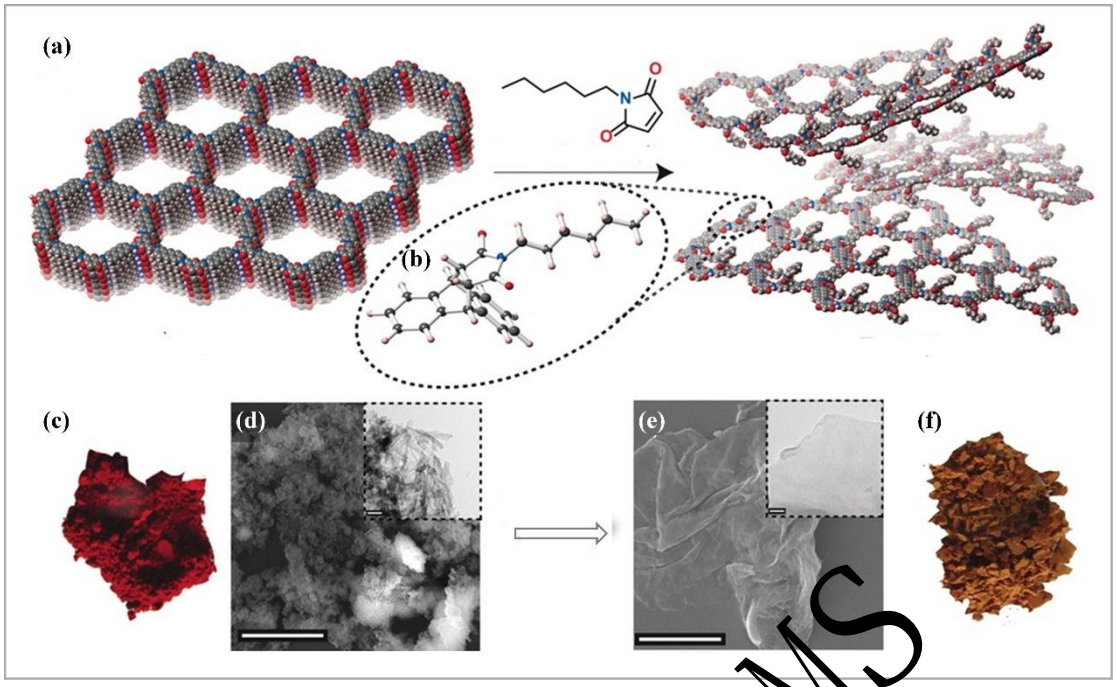

Fig. 8 (a) Schematic representation of the chemical exfoliation of DaTp to DaTp-CONs. (b) Energy-optimized structure of the cycloadduct of N-hexylmaleimide and anthracene. (c) Optical image of DaTp. (d) SEM image (5 µm) of DaTp with an inserted TEM image (100 nm). (e) SEM image (5 µm) of DaTp-CONs with an inserted TEM image (100 nm). (f) Optical image of DaTp-CONs. Reproduced with permission from ref. 101. Copyright 2016, Wiley-VCH.

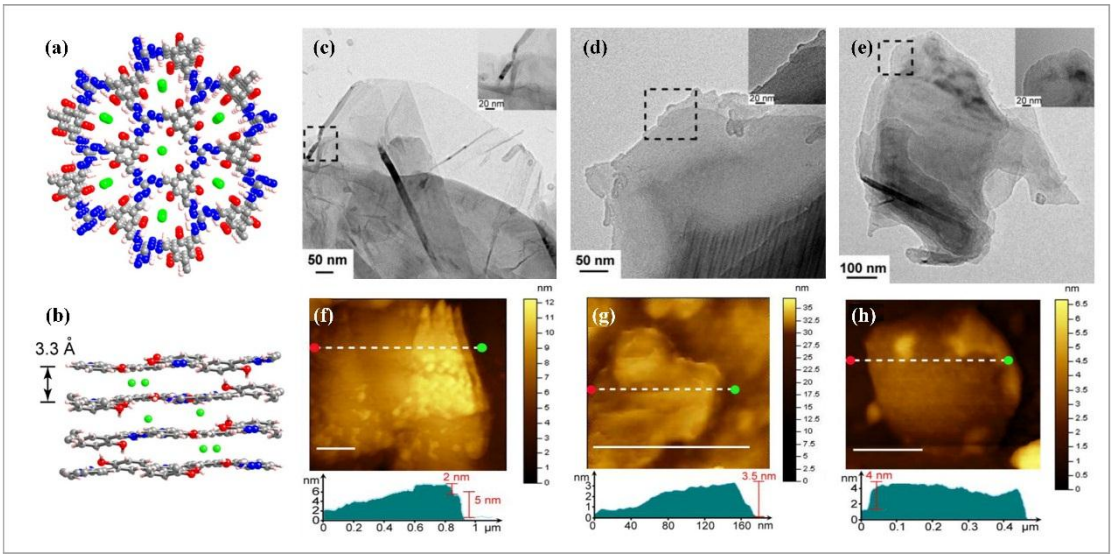

Fig. 9 (a) Modeling of TpTGCl in eclipsed mode (top view). (b) Stacking model showing individual layers (side view). (c–e) TEM images of TpTGCl, TpTGBr, and TpTGI, respectively (inset shows zoomed in images; scale bar = 20 nm). (f–h) AFM images and height profile of TpTGCl, TpTGBr, and TpTGI, respectively (AFM scale bars represent 200 nm). Reproduced with permission from ref. 107. Copyright 2016, American Chemical Society.

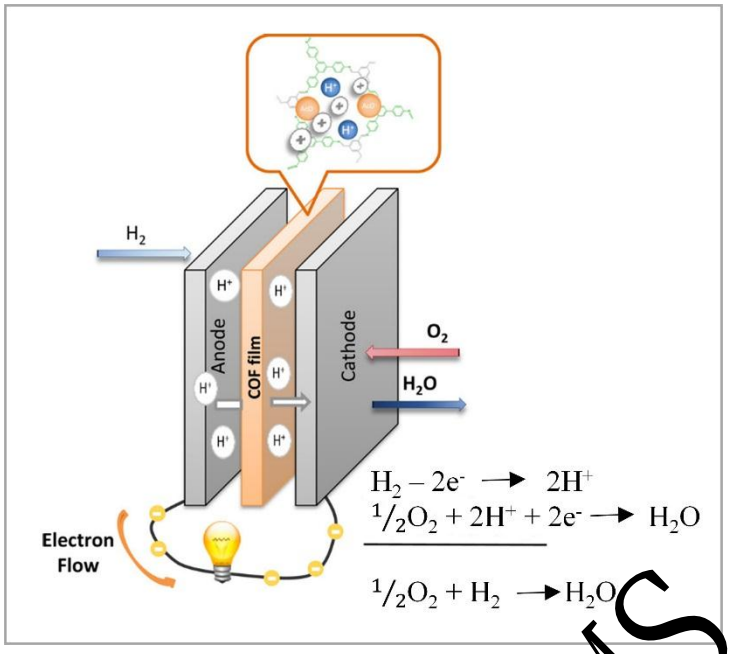

Fig. 10 Schematic representation of the PEMFCs with the membrane electrode assemblies (MEA) of RT-COF-1Ac, RT-COF-1AcB, and LiCl@RT-COF-1 films. Reproduced with permission from ref. 122. Copyright 2017, American Chemical Society.

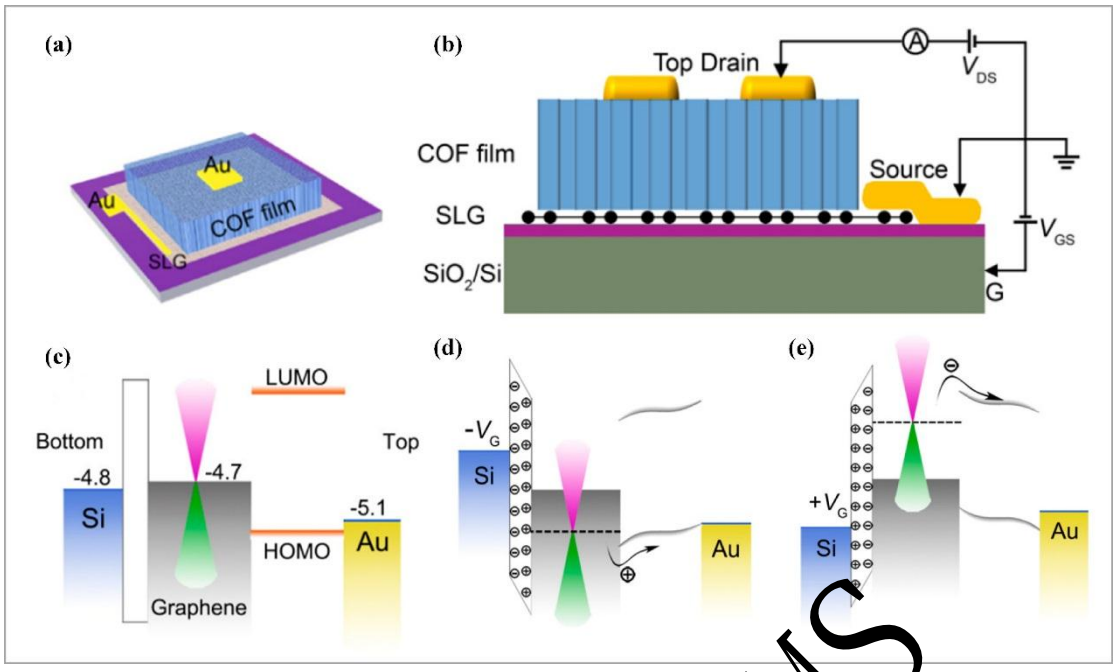

Fig. 11 (a) $COF_{TFPy\text{-}PPDA}$ film on SLG/SiO_2–Si. (b) Module of the constructed COF/SLG-VFET device (side view). (c) The relevant levels of materials in the SLG/COF-VFET and the band diagrams in the case of (d) negative gate voltage and (e) positive gate voltage. Reproduced with permission from ref. 135. Copyright 2017, American Chemical Society.

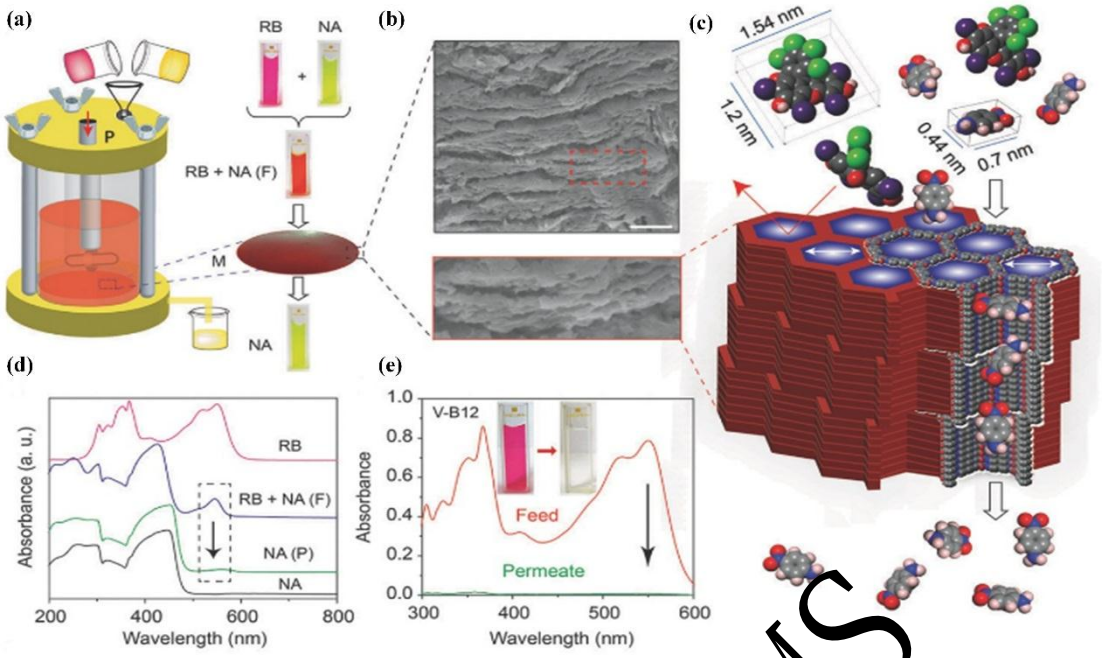

Fig. 12 (a) Schematic representation of the nanofiltration assembly in the case of selective molecular separation of nitroaniline (NA) from a mixture of NA and rose Bengal (RB), ("F" denotes feed and "P" for permeate). (b) Cross-sectional SEM image of M-TpBD thin film (Scale bar 10 µm). (c) Schematic representation of molecular sieving mechanism for M-TpBD. (d) UV–vis spectra related to the selective recovery of NA from mixture of RB and NA from water. (e) UV–vis spectra of vitamin-B12 (V-B12) and the filtrate water after passing through M-TpBD. Reproduced with permission from ref. 153. Copyright 2017, Wiley-VCH.

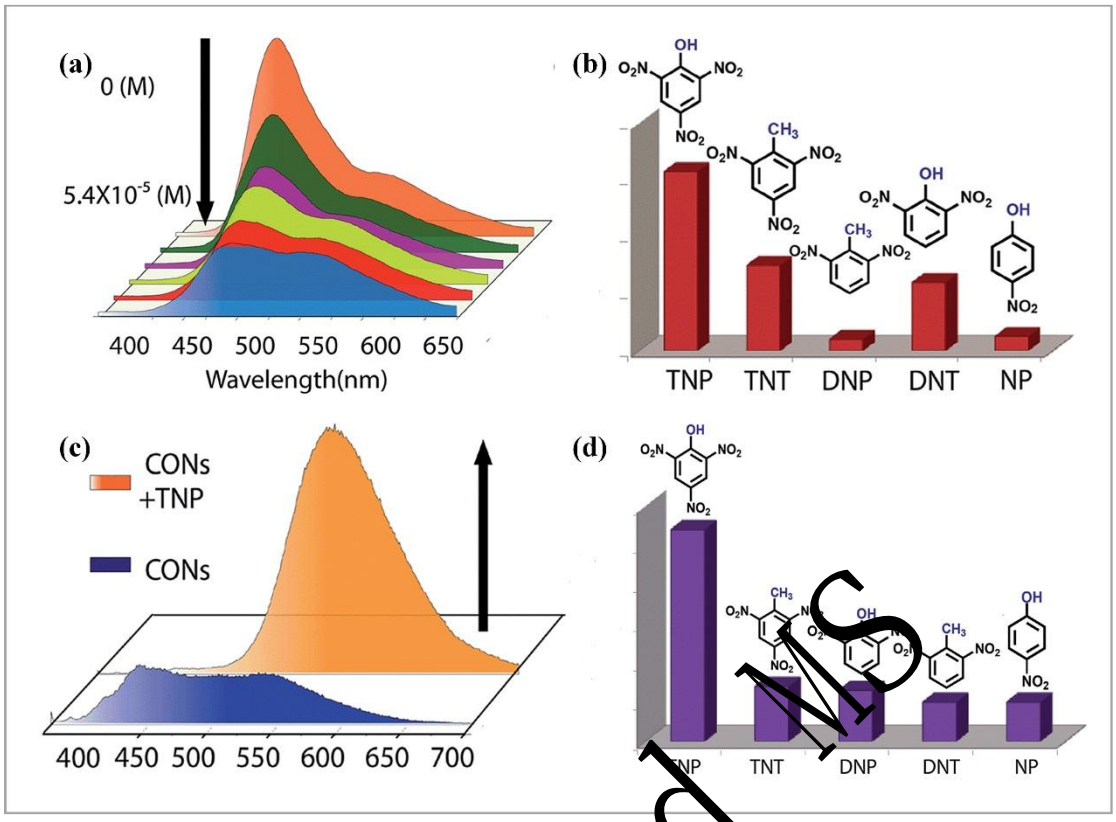

Fig. 13 (a) PL quenching of "Turn-off" sensing in solution phase. (b) Selectivity of TfpBDH-CONs towards analytes based on Fluorescence quenching. (c) PL enhancement of "turn-on" sensing in solid phase. (d) Selectivity of TfpBDH-CONs towards analytes based on Fluorescence enhancement. Reproduced with permission from ref. 177. Copyright 2015, Royal Society of Chemistry.

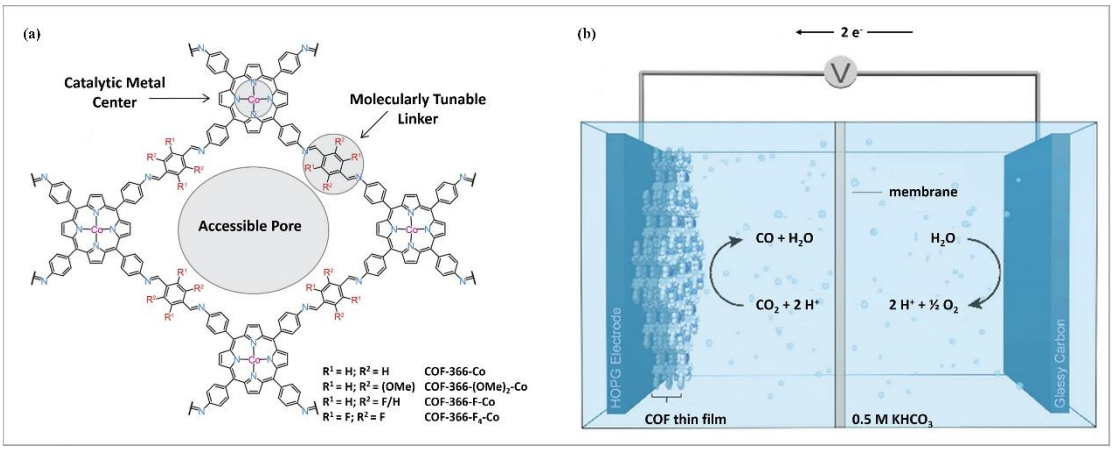

Fig. 14 (a) Structure of Cobalt-porphyrin based COF backbone. (b) Schematic illustration of electrolysis cell electrocatalytic CO_2 reduction. Reproduced with permission from ref. 182. Copyright 2018, American Chemical Society.